



**CIVIL ENGINEERING STUDIES**

Illinois Center for Transportation Series No. 21-030

UIIU-ENG-2021-2030

ISSN: 0197-9191

# **High-volume Fly Ash Concrete for Pavements Findings: Volume 1**

Prepared By

**Aniruddha Baral**

**Jeffrey R. Roesler**

University of Illinois at Urbana-Champaign

**M. Tyler Ley**

**Shinhyu Kang**

**Loren Emerson**

**Zane Lloyd**

**Braden Boyd**

**Marllon Dan Cook**

Oklahoma State University

Research Report No. FHWA-ICT-21-025

A report of the findings of

**ICT PROJECT R27-180**

**Concrete Pavement Mixtures with High Supplementary Cementitious Materials (SCM) Content**

<https://doi.org/10.36501/0197-9191/21-030>

---

**Illinois Center for Transportation**

**September 2021**



**TECHNICAL REPORT DOCUMENTATION PAGE**

<b>1. Report No.</b> FHWA-ICT-21-025		<b>2. Government Accession No.</b> N/A		<b>3. Recipient's Catalog No.</b> N/A	
<b>4. Title and Subtitle</b> High-volume Fly Ash Concrete for Pavements Findings: Volume 1				<b>5. Report Date</b> September 2021	
				<b>6. Performing Organization Code</b> N/A	
<b>7. Authors</b> Aniruddha Baral ( <a href="https://orcid.org/0000-0003-0810-5475">https://orcid.org/0000-0003-0810-5475</a> ), Jeffery R. Roesler ( <a href="https://orcid.org/0000-0001-6194-269X">https://orcid.org/0000-0001-6194-269X</a> ), M. Tyler Ley				<b>8. Performing Organization Report No.</b> ICT-21-030 UILU-2021-2030	
<b>9. Performing Organization Name and Address</b> Illinois Center for Transportation Department of Civil and Environmental Engineering University of Illinois at Urbana-Champaign 205 North Mathews Avenue, MC-250 Urbana, IL 61801				<b>10. Work Unit No.</b> N/A	
				<b>11. Contract or Grant No.</b> R27-180	
<b>12. Sponsoring Agency Name and Address</b> Illinois Department of Transportation (SPR) Bureau of Research 126 East Ash Street Springfield, IL 62704				<b>13. Type of Report and Period Covered</b> Final Report 10/1/17–9/30/21	
				<b>14. Sponsoring Agency Code</b>	
<b>15. Supplementary Notes</b> Conducted in cooperation with the U.S. Department of Transportation, Federal Highway Administration. <a href="https://doi.org/10.36501/0197-9191/21-030">https://doi.org/10.36501/0197-9191/21-030</a>					
<b>16. Abstract</b> High-volume fly ash concrete (HVFAC) has improved durability and sustainability properties at a lower cost than conventional concrete, but its early-age properties like strength gain, setting time, and air entrainment can present challenges for application to concrete pavements. This research report helps with the implementation of HVFAC for pavement applications by providing guidelines for HVFAC mix design, testing protocols, and new tools for better quality control of HVFAC properties. Calorimeter tests were performed to evaluate the effects of fly ash sources, cement–fly ash interactions, chemical admixtures, and limestone replacement on the setting times and hydration reaction of HVFAC. To better target the initial air-entraining agent dosage for HVFAC, a calibration curve between air-entraining dosage for achieving 6% air content and fly ash foam index test has been developed. Further, a digital foam index test was developed to make this test more consistent across different labs and operators. For a more rapid prediction of hardened HVFAC properties, such as compressive strength, resistivity, and diffusion coefficient, an oxide-based particle model was developed. An HVFAC field test section was also constructed to demonstrate the implementation of a noncontact ultrasonic device for determining the final set time and ideal time to initiate saw cutting. Additionally, a maturity method was successfully implemented that estimates the in-place compressive strength of HVFAC through wireless thermal sensors. An HVFAC mix design procedure using the tools developed in this project such as the calorimeter test, foam index test, and particle-based model was proposed to assist engineers in implementing HVFAC pavements.					
<b>17. Key Words</b> Concrete, Fly Ash, Hydration, Cementitious Material, Maturity, Setting Time, Limestone, Particle Group, Foam Index, Maturity, Noncontact Ultrasound			<b>18. Distribution Statement</b> No restrictions. This document is available through the National Technical Information Service, Springfield, VA 22161.		
<b>19. Security Classif. (of this report)</b> Unclassified		<b>20. Security Classif. (of this page)</b> Unclassified		<b>21. No. of Pages</b> 46	<b>22. Price</b> N/A



# ACKNOWLEDGMENT, DISCLAIMER, MANUFACTURERS' NAMES

This publication is based on the results of **ICT-R27-180: Concrete Pavement Mixtures with High Supplementary Cementitious Materials (SCM) Content**. ICT-R27-180 was conducted in cooperation with the Illinois Center for Transportation; the Illinois Department of Transportation; and the U.S. Department of Transportation, Federal Highway Administration.

Members of the Technical Review Panel (TRP) were the following:

- James Krstulovich, TRP Chair, Illinois Department of Transportation
- Dennis Bachman, Federal Highway Administration
- Darrin Davis, Illinois Department of Transportation
- Kevin Finn, Illinois Department of Transportation
- Dan Gancarz, Applied Research Associates, Inc.
- Stephen Jones, Illinois Department of Transportation
- Kelly Morse, Illinois Department of Transportation
- Chad Pink, Illinois Department of Transportation
- Megan Swanson, Illinois Department of Transportation
- Dan Tobias, Illinois Department of Transportation
- Melinda Winkelman, Illinois Department of Transportation
- Steve Worsfold, Illinois Department of Transportation

The contents of this report reflect the view of the authors, who are responsible for the facts and the accuracy of the data presented herein. The contents do not necessarily reflect the official views or policies of the Illinois Center for Transportation, the Illinois Department of Transportation, or the Federal Highway Administration. This report does not constitute a standard, specification, or regulation.

Trademark or manufacturers' names appear in this report only because they are considered essential to the object of this document and do not constitute an endorsement of product by the Federal Highway Administration, the Illinois Department of Transportation, or the Illinois Center for Transportation.

## EXECUTIVE SUMMARY

High-volume fly ash concrete (HVFAC) has improved durability and sustainability properties at a lower cost than conventional concrete, but its early-age properties like strength gain, setting time, and air entrainment can present challenges for application to concrete pavements. This research report helps with the implementation of HVFAC for pavement applications by providing guidelines for HVFAC mix design, testing protocols, and new tools for better quality control of HVFAC properties. Calorimeter tests were performed to evaluate the effects of fly ash sources, cement–fly ash interactions, chemical admixtures, and limestone replacement on the setting times and hydration reaction of HVFAC. To better target the initial air-entraining agent dosage for HVFAC, a calibration curve between air-entraining dosage for achieving 6% air content and fly ash foam index test was developed. Further, a digital foam index test was developed to make this test more consistent across different labs and operators. For a more rapid prediction of hardened HVFAC properties, such as compressive strength, resistivity, and diffusion coefficient, an oxide-based particle model was developed. An HVFAC field test section was also constructed to demonstrate the implementation of a noncontact ultrasonic device for determining the final set time and ideal time to initiate saw cutting. Additionally, a maturity method was successfully implemented that estimates the in-place compressive strength of HVFAC through wireless thermal sensors. An HVFAC mix design procedure using the tools developed in this project such as the calorimeter test, foam index test, and particle-based model was proposed to assist engineers in implementing HVFAC pavements.

The research findings are described in detail in two main reports (volumes 2 and 3), with volume 1 summarizing the significant research findings and implementable outcomes for the research effort. Research performed by the University of Illinois at Urbana-Champaign was discussed in volume 2 as well as details and findings of the HVFAC literature review, quarterly variability of fly ash sources, effect of limestone and different chemical admixtures on the hydration of HVFAC, development of a digital foam index test, and implementation of the maturity method and noncontact ultrasound setting time device in the field. Research performed by Oklahoma State University was discussed in volume 3, with details and findings of compressive strength, slump, and resistivity of HVFAC mixes.

# TABLE OF CONTENTS

<b>CHAPTER 1: INTRODUCTION AND RESEARCH GAPS .....</b>	<b>1</b>
<b>CHAPTER 2: HVFAC EARLY-AGE PROPERTIES.....</b>	<b>3</b>
<b>CHARACTERIZATION TESTS .....</b>	<b>3</b>
<b>AIR ENTRAINMENT.....</b>	<b>3</b>
Foam Index vs. AEA Dosage Requirement in Concrete .....	4
Digital Foam Index Test .....	6
<b>SETTING TIME.....</b>	<b>9</b>
Effect of Chemical Admixtures on Setting Time .....	11
Set Time Acceleration with Limestone .....	12
Noncontact Ultrasound Device for Setting Time Measurement .....	17
<b>STRENGTH .....</b>	<b>19</b>
Calorimeter Tests .....	19
Concrete Strength Test .....	20
<b>CHAPTER 3: PARTICLE MODEL FOR HVFAC STRENGTH DEVELOPMENT AND DURABILITY ....</b>	<b>24</b>
<b>PARTICLE MODEL TO PREDICT COMPRESSIVE STRENGTH .....</b>	<b>25</b>
<b>PARTICLE MODEL TO PREDICT DIFFUSION COEFFICIENT .....</b>	<b>26</b>
<b>PARTICLE MODEL TO PREDICT RESISTIVITY FOR HVFAC.....</b>	<b>27</b>
<b>COMPARING RESISTIVITY AND DIFFUSION COEFFICIENT .....</b>	<b>28</b>
<b>RECOMMENDATIONS FOR ASR / SALT SCALING / FREEZE-THAW BASED ON THE LITERATURE     REVIEW .....</b>	<b>31</b>
<b>CHAPTER 4: FIELD IMPLEMENTATION OF HVFAC.....</b>	<b>32</b>
<b>FIELD MATURITY METHOD FOR STRENGTH.....</b>	<b>32</b>
In-place Strength Estimation Using Maturity Method .....	34
<b>NONCONTACT ULTRASOUND SETTING TIME TEST METHOD.....</b>	<b>35</b>
<b>SAW CUTTING .....</b>	<b>36</b>
<b>CHAPTER 5: MIX DESIGN ACCOMODATIONS FOR HVFAC .....</b>	<b>38</b>
<b>STEP 1: OXIDE ANALYSIS AND STRENGTH PREDICTION .....</b>	<b>38</b>
<b>STEP 2: AEA DOSAGE REQUIREMENT .....</b>	<b>38</b>

**STEP 3: CALORIMETER RESPONSE ..... 38**  
**STEP 4: TRIAL MIX DESIGN AND ADJUSTMENTS..... 39**  
**CHAPTER 6: SUMMARY AND RECOMMENDATIONS ..... 40**  
**REFERENCES ..... 42**



# LIST OF FIGURES

Figure 1. Photos. Image of foam layer with (a) little to no coverage of container surface and (b) foam layer covering entire container surface. .... 4

Figure 2. Graph. Number of drops to reach foam index versus loss on ignition. .... 5

Figure 3. Graph. AEA dosage vs. the number of drops to reach foam index. .... 5

Figure 4. Photos. Digital foam index test setup (a) consisting of a video camera, foam index container, and a laptop for data storage. A representative image of the foam layer is shown in (b) with the empty area manually annotated. .... 6

Figure 5. Graphs. Change in empty area fraction with time (a) for different AEA dosage additions for a representative fly ash sample (fly ash 3). The evolution of empty area with number of drops of AEA addition for different times after stopping the shaking is shown in (b). Both figures use the same digital foam index test data. .... 8

Figure 6. Graphs. AEA dosage required for making the foam layer stable and the foam index for different ashes with different LOIs (a). The ratio of foam index and AEA dosage required for making the foam layer stable is plotted in (b). .... 9

Figure 7. Graph. Isothermal calorimetry results for a sample Portland cement with initial and final setting times of 3.3 hours and 6.5 hours, respectively. .... 10

Figure 8. Graphs. Effect of superplasticizer and water reducer on heat flow rates for 40% weight replacement of cement with (a) Fly Ash 1 (Class C), (b) Fly Ash 4 (Class F) for 2019 quarter 2 samples.. 12

Figure 9. Graphs. Effect of increasing micro-limestone replacement on heat flow rates for 40% weight replacement of cement with (a) Fly Ash 1 (Class C), (b) Fly Ash 4 (Class F) for 2019 quarter 2 samples.. 14

Figure 10. Graphs. Effect of increasing nano-limestone replacement on heat flow rates for 40% weight replacement of cement with (a) Fly Ash 1 (Class C), (b) Fly Ash 4 (Class F) for 2019 quarter 2 samples.. 15

Figure 11. Graphs. Effect of superplasticizer and water reducer on heat flow rates for 5% micro-limestone and 40% weight replacement of cement with (a) Fly Ash 1 (Class C), (b) Fly Ash 4 (Class F) for 2019 quarter 2 samples..... 16

Figure 12. Schematic. Leaky Rayleigh wave propagation in concrete at different stages of hydration. 18

Figure 13. Schematic. Noncontact ultrasound setting time measurement device. .... 18

Figure 14. Graphs. Effect of superplasticizer and water reducer on cumulative heat flow for 40% weight replacement of cement with (a) Fly Ash 1 (Class C), (b) Fly Ash 4 (Class F) for 2019 quarter 2 samples. .... 20

Figure 15. Graph. Comparison of slumps measured for each fly ash mixture at 20% and 40% replacement levels with the control (OPC). .... 21

Figure 16. Graph. 20% fly ash mixtures compressive strength as a percent of the control at 3 and 90 days of hydration. .... 22

Figure 17. Graph. 40% fly ash mixtures compressive strength as a percent of the control at 3 and 90 days of hydration. .... 23

Figure 18. Photo. The comprehensive procedure of the particle model. .... 24

Figure 19. Graphs. Relationship between the predicted and measured strength by using the particle model for (a) 20% fly ash concrete and (b) 40% fly ash concrete for ages 3 to 180 days..... 25

Figure 20. Graphs. Comparison between the calculated and measured values for  $D_{ic}$ . .... 27

Figure 21. Graphs. Comprehensive relationship between the calculated and experimental resistivity for (a) 20% fly ash replacement and (b) 40% fly ash replacement. .... 28

Figure 22. Equation. Nernst-Einstein equation. .... 28

Figure 23. Graphs. Comprehensive correlation between  $\rho_{sr}$  and  $D_{ic}$  for samples with fly ash and OPC. .... 29

Figure 24. Graphs. All comparisons for 20% and 40% fly ash replacement with +30% limit line and  $K_s$ . Lines are also included to show an example of using the  $K_s$  relationship..... 31

Figure 25. Photo. HVFAC field pavement test section details (not to scale). .... 32

Figure 26. Graph. Compressive strength vs. age for control and HVFA concrete mixes. .... 33

Figure 27. Graph. Laboratory maturity calibration curve for HVFAC and control mixes. .... 34

Figure 28. Photo. Noncontact ultrasound setting time measurement device at the field test site. .... 35

Figure 29. Graphs. Leaky Rayleigh wave energy of the (a) control concrete and (b) HVFAC mixes..... 36

Figure 30. Photos. Saw cut and joint raveling in (a) control and (b and c) HVFAC sections..... 37

## LIST OF TABLES

Table 1. Effect of Chemical Admixtures on Setting Times of HVFAC (Cement A + 40% Fly Ash).....	12
Table 2. Effect of Limestone Replacement of Cement on Setting Time of HVFA Mixes .....	15
Table 3. Effect of Superplasticizer and Water Reducer on Setting Times for 5% Micro-limestone and 40% Weight Replacement of Cement with Different Fly Ash Sources .....	17
Table 4. Effect of 5% Micro-limestone Replacement on the Acceleration of Setting Times.....	17
Table 5. Final Setting Time Comparison between Noncontact Ultrasound Device and Isothermal Calorimeter.....	19
Table 6. Mixture Designs.....	21
Table 7. Summary of K and R-squared Values for All Investigations.....	30
Table 8. Mix Design and Fresh Properties of Control and HVFA Concrete Mixes .....	33
Table 9. In-place Compressive Strength of the HVFAC Mix in the Field.....	34
Table 10. Final Setting Time of HVFAC and Control Mixes in the Laboratory .....	36
Table 11. Mixture Property Adjustment Strategies for HVFAC Mixtures (Listed in Order of Importance) .....	39



# CHAPTER 1: INTRODUCTION AND RESEARCH GAPS

Replacing cement with supplementary cementitious materials (SCMs) has been practiced for decades, with the primary objectives being to reduce the concrete material unit cost and increase material durability. More recently, improving the sustainability of concrete has encouraged discussion on even higher replacement levels of cement with SCMs. SCMs can include multiple products such as fly ash, slag, calcined clay, and different natural pozzolans, but fly ash and slags are used most frequently and will be investigated in this project. Illinois Department of Transportation (IDOT) currently allows a maximum 25%, 30%, and 35% cement replacement with Class F fly ash, Class C fly ash, and ground granulated blast furnace slag (GGBFS), respectively. As application up to 50% GGBFS is allowed by multiple agencies in the United States (California Department of Transportation 2013; Federal Aviation Administration 2018), this study focused on investigating high-volume fly ash concrete (HVFA) for pavements.

Some of the specific performance benefits of partial replacement of cement with fly ash are mitigating the alkali-silica reaction (Detwiler 1997), decreasing ion permeability (Yurdakul et al. 2014), improving joint deterioration susceptibility (Farnam, Zhang, and Weiss 2017; Suraneni et al. 2017), and lowering the heat of hydration of mass concrete (Bamforth 1980). The Federal Highway Administration and several state transportation agencies (e.g., Caltrans, Indiana Department of Transportation, etc.) have already initiated research on this topic (Nassif and Suksawang 2003; Tanikella and Olek 2017). Existing literature demonstrates that a high rate of replacement by fly ash (40% to 65%) is possible while still meeting the long-term strength criteria. Although many advantages exist for concrete mixtures with a higher volume of fly ash, early-age properties such as air content, setting times, and strength gain rates can be affected (Taylor et al. 2006a), which can limit the permissible replacement levels.

The influence of fly ash on concrete's early-age properties depends on the chemical composition of the crystalline and amorphous phases, volume replacement level, and particle size. Restrictions on fly ash use based on broad oxide contents or arbitrary replacement levels can lead to missed opportunities, which can improve both the cost and durability of concrete pavements. With the urgency to apply higher replacement levels of fly ash in concrete pavements, rapid advanced characterization techniques of the fly ash coupled with mineral and chemical admixtures can provide the appropriate testing protocols and mixture modifications to enable the use of HVFA, i.e., cement replacement rates of 40% or higher. The use of HVFA is particularly challenging in pavement applications because of lower set times, lower strength gain, and air-entrainment issues. The durability performances such as the alkali-silica reaction and corrosion resistance of HVFA are generally adequate for pavement applications, but the durability properties need to be verified for fly ash available in Illinois. Moreover, the variability of fly ash obtained from the same source over time may require diligent quality control.

This report focuses on five research areas for implementing HVFA mixes in concrete pavements. First, setting time and early-age hydration are evaluated using calorimeter along with compositional characterization tests of the fly ash. The effect of different mix design variables such as chemical admixtures, cement-fly ash interactions, and use of limestone to accelerate setting time of HVFA

are evaluated. Second, a foam index test is used for determining air-entraining dosage requirement of concrete. A computer-based digital foam index test is also developed for better operator repeatability. Third, a model is developed to predict the compressive strength, resistivity, and diffusion coefficient of HVFAC based on the particle-based oxide content of the fly ash. Fourth, a HVFAC field pavement test section is constructed to demonstrate the usage of the maturity method for determination of in-place compressive strength as well as application of a noncontact ultrasound device for final set determination in the field. Fifth, a mixture design process is suggested for developing HVFAC for pavements. Finally, recommendations are provided that can be incorporated into IDOT's standard practices when using HVFAC in pavements.

## **CHAPTER 2: HVFAC EARLY-AGE PROPERTIES**

### **CHARACTERIZATION TESTS**

The current characterization tests in ASTM C618 should continue to be run with the replacement of the loss on ignition (LOI) with the foam index test, which is outlined in this document and volume 2 (Baral, Roesler, and Fu 2021). The foam index test employed in this project does not exactly match the one described in ASTM C1827. For higher volume fly ash mixtures, e.g., 30% to 40%, isothermal calorimetry testing should be completed following ASTM C1702's guidance for the mixture of cement, fly ash, and admixtures. This will give insights into the setting time of the mixture. This information can be used to educate the producer, contractor, and agency (IDOT) about the set time and the early-age strength development of the mixture. This can be determined by completing calorimetry testing with cement only, typical fly ash dosage (20% replacement of cement), HVFA (40% replacement), HVFA (40% replacement with admixtures), and then comparing the heat flow curves, maximum rate of heat release, and set time values. It is critical that admixtures are included in the calorimeter tests because they play a significant role in the set time and early strength gain of HVFA mixtures. It is also desirable to complete a trial batch of the mixture. More details will be discussed on HVFAC trial batches in Chapter 5.

### **AIR ENTRAINMENT**

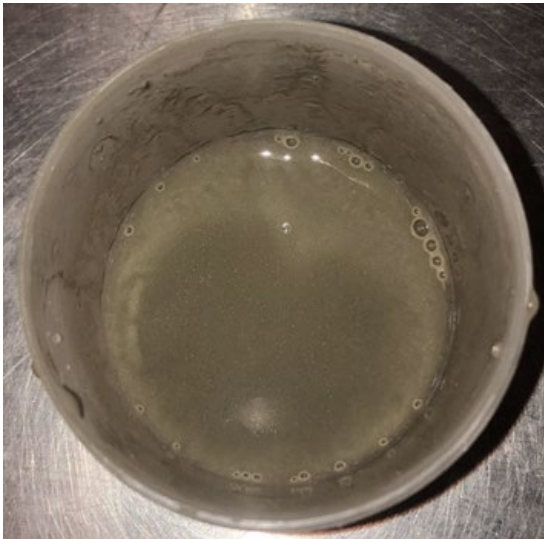
The durability of concrete is dependent on the ability to withstand environmental effects. One of the major factors leading to infrastructure cracking is freeze-thaw damage in concrete. Research (Jin, Zhang, and Huang, 2013) has shown that to resist damage from cyclic freeze-thaw, small and well-distributed air-void systems are necessary for concrete. Obtaining a concrete mixture with a desired air-void distribution requires the addition of an air-entraining agent (AEA) to the concrete. The damage inflicted on concrete from cycles of freezing and thawing can be mitigated with effective air-void spacing. The use of air-entraining agents will encourage the formation of stable air voids in the concrete mixture of the right size and spacing as well as prevent these bubbles from coalescing. The desired volume to prevent cracking from freezing and thawing cycles for normal concrete pavement mixtures is approximately 6% of the concrete volume.

When designing admixture dosage, it is common practice to make a trial mixture to adjust the design of the concrete mixture. The use of AEAs has proven difficult in characterizing dosage proportions (Ley et al. 2008). A primary factor that affects the AEA dosage is the impact of carbon within fly ash to absorb the AEA (Ley et al. 2008). The addition of fly ash can cause difficulty in the entrainment of air for a concrete mixture. The residual unburned carbon content in fly ash will adsorb the AEA and create challenges during the process to increase the air content (American Coal Ash Association 2003).

Simple tests are needed to determine how fly ash impacts the air-entrainment dosage in concrete. The foam index test is a rapid test method that has the potential to predict the AEA demand for fly ash (Harris et al. 2008a, 2008b, 2008c; Ley et al. 2008).

## Foam Index vs. AEA Dosage Requirement in Concrete

There are many versions of the foam index test, but systematic research has been done to find a useful vessel volume, material ratios, and fluid content to provide the best correlation to concrete (Harris et al. 2008a, 2008b, 2008c; Ley et al. 2008). In this research, the foam index test uses a 125 mL (4.23 oz) container partially filled with 5 g (0.176 oz) of cement, 5 g (0.176 oz) of fly ash, and 25 mL (0.845 oz) of potable water. The container was sealed with a lid and shaken for 20 seconds. A mixture of distilled water and 2.5% wood resin AEA solution is added with a dropper in increments of two to five drops at a time and then shaken for 10 seconds. The dropper can be weighed before and after adding the drops to determine how much material is added. The ability of the fly ash to maintain a steady foam on the surface is considered the foam index value and the volume of AEA added per gram of fly ash is quantitatively used to compare different mixtures. Figure 1 presents a comparison of the expected behavior of the foam at the beginning and end of the test. The foam index test can be run at the ready-mix plant or in the field for quality control of the fly ash.



A. Foam covering little / no container surface



B. Foam covering entire container surface

**Figure 1. Photos. Image of foam layer with (a) little to no coverage of container surface and (b) foam layer covering entire container surface.**

Figure 2 presents the correlation between the LOI results and the drops of AEA required to reach stable foam. The results show that there is essentially no correlation between the LOI test and the AEA demand. A limit of 6% LOI has also been added to the figure to show the typical limit allowed by ASTM C618. Three fly ash samples in this study exceeded the 6% LOI limit; however, the AEA demand to reach a stable foam is not significantly higher than the fly ash within the 6% LOI limit. This shows that the LOI limit may not be a useful indicator of performance of the AEA requirement of fly ash. The use of a performance-based test like the foam index will allow fly ash to be characterized prior to trial batching and determination of the initial AEA dosage.



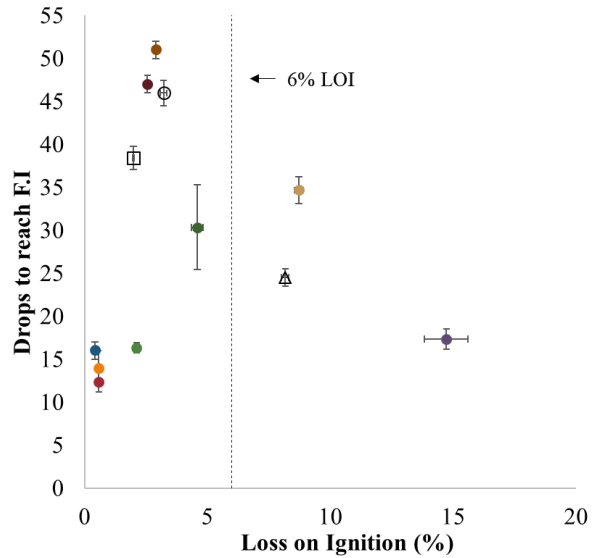


**Figure 2. Graph. Number of drops to reach foam index versus loss on ignition.**

Figure 3 compares the AEA dosage for achieving 6% air content in concrete and the amount of diluted AEA required in the foam index test. The value of 6% air content was used because it is the most common value used in concrete specifications. The trend line for the points in Figure 3 show an R-squared value greater than 0.90; the data shows good agreement between the AEA dosage for concrete mixtures with different fly ash sources and the number of drops required to reach a stable foam. The data in Figure 3 also shows that the use of the foam index test to predict the AEA dosage requirement for a concrete mixture of 6% air content is applicable. This means the foam index is a valuable and simple test method to evaluate the AEA demand in normal concrete and HVFAC mixtures.

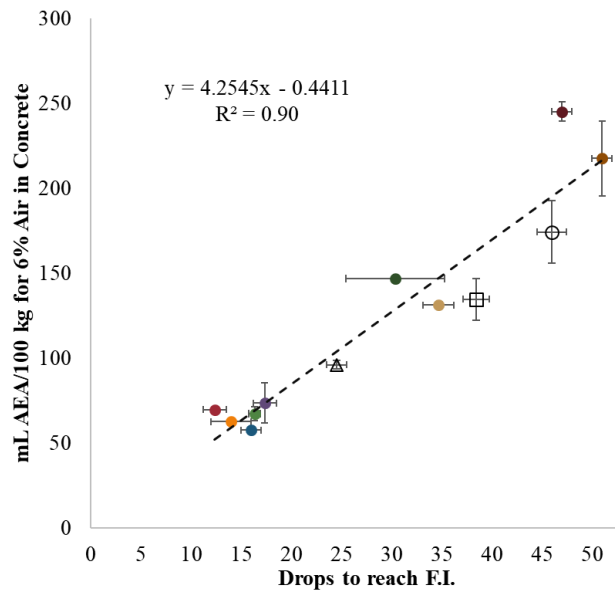


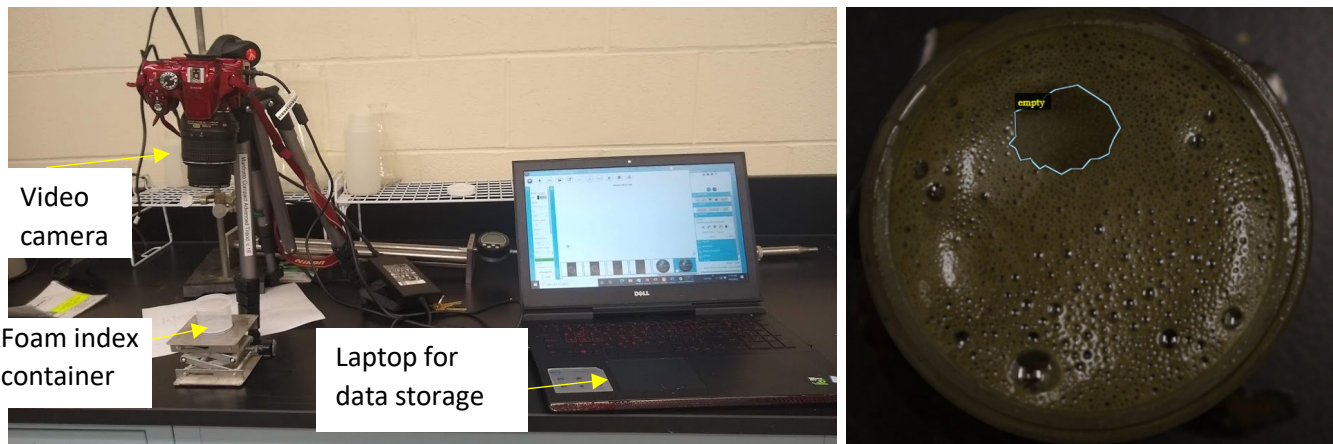
**Figure 3. Graph. AEA dosage vs. the number of drops to reach foam index.**

This research has shown that the fly ash can change the AEA demand by approximately four times for a given concrete. This high variability is problematic for concrete producers in terms of both cost of admixture as well as challenges with consistent AEA dosages. Previous studies have shown an ability to use the foam index test to predict the amount of AEA dosage required for different fly ash mixtures (Ley et al. 2008). By testing new fly ash with the foam index test, the impact the AEA dosage has on air content can be predicted. This provides a dependable preliminary AEA dosage in concrete to reach the desired air content that is more reliable than the existing LOI test.

## Digital Foam Index Test

Since the introduction of the foam index test about 30 years ago, researchers have studied (Harris et al. 2008a, 2008b, 2008c) the effects of different test parameters such as water-to-binder ratio, fly ash-to-binder ratio, container capacity versus the amount of solution used, mixing procedure, time of test, etc. and proposed guidelines for a standardized test method given its known repeatability issues (Taylor et al. 2006a, 2006b). One of the major reasons behind the repeatability issues of the foam index test is that human judgment is used to know whether the foam has covered the surface fully, leading to errors. Here we propose using a computer vision technique to determine when the foam is stable and has covered the entire solution surface, and thus reduce operator error and improve consistency between laboratories. Moreover, this test can provide insights regarding the fly ash AEA interaction mechanisms.

This procedure employs the traditional foam index test method but also takes a video of the created foam layer with a digital camera. A neural network–based computer vision algorithm has been used to detect the empty area (i.e., area not covered by the foam on the container surface) and surface area covered by the foam. The empty area detected by the algorithm was normalized by the bottle cross-sectional area to obtain the “empty area fraction” parameter. Figure 4 presents the digital foam index test setup.



A. Video camera, foam index container, and a laptop

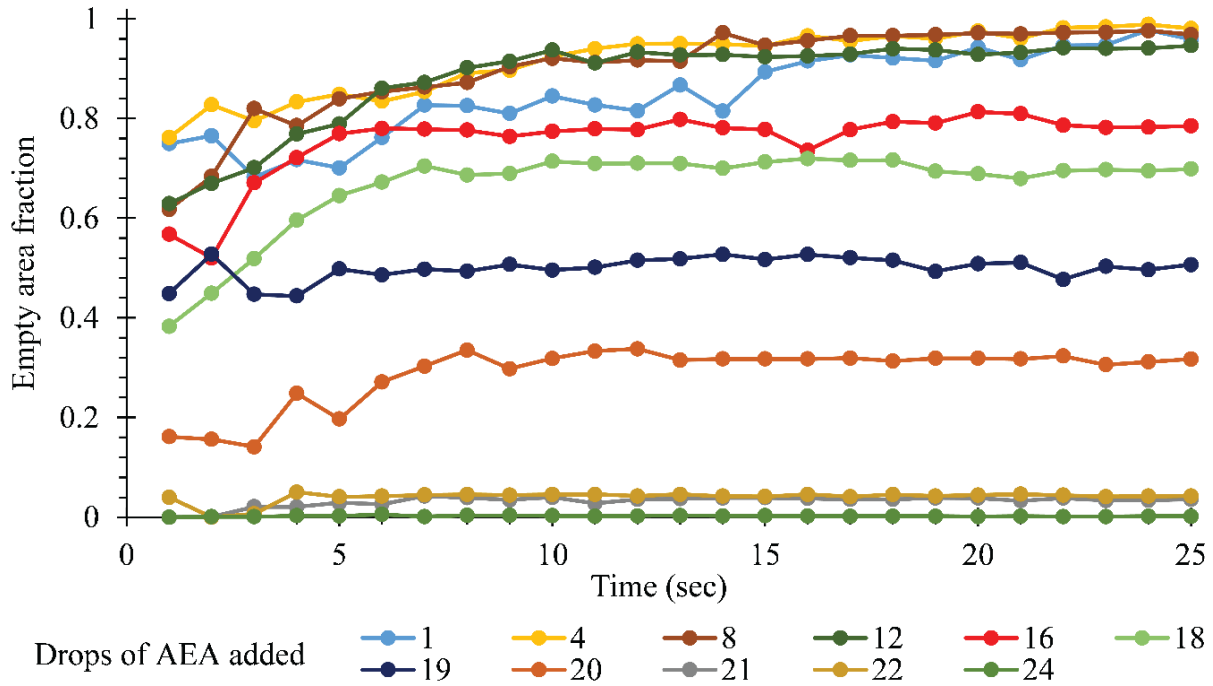
B. Image of the foam layer

**Figure 4. Photos. Digital foam index test setup (a) consisting of a video camera, foam index container, and a laptop for data storage. A representative image of the foam layer is shown in (b) with the empty area manually annotated.**

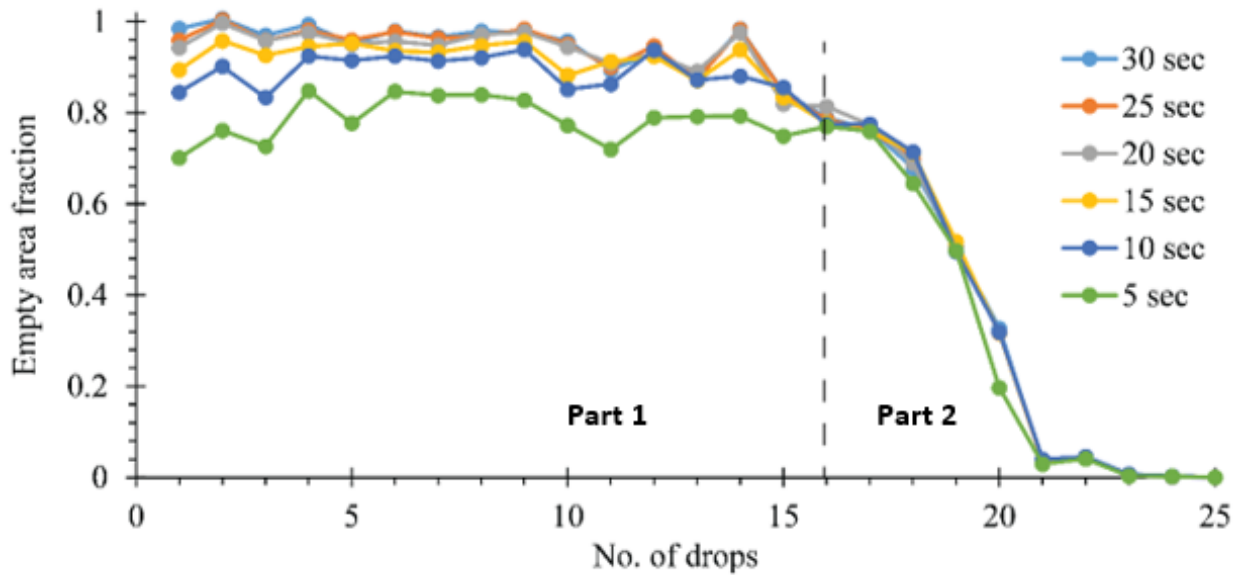
*Source: Baral, Roesler, and Fu (2021)*

The results of the digital foam index test of a representative fly ash sample are presented in Figure 5 with the foam layer covering the entire container surface after adding 24 drops of AEA (2.4  $\mu\text{L}$  AEA/gm). The empty area fraction measured after 20 seconds of shaking decreases with increasing AEA dosage until it becomes zero (Figure 5-A). To further understand the effect of AEA dosage on the evolution of empty area fraction with time, the data in Figure 5-A was replotted with empty area fraction on the y-axis and number of drops of AEA on the x-axis (Figure 5-B). The empty area fraction did not change with time (time > 5 seconds) after 16 drops of AEA addition, showing that the foam layer becomes stable only after 16 drops of AEA addition (part 1), even though it takes 24 drops to make the foam layer cover the entire container surface (foam index, part 2). A stable foam occurs first with fewer AEA drops as compared to the total number drops to make a stable foam and cover the entire container surface area (i.e., foam index). In other words, after addition of certain amount of AEA dosage (part 1), the foam layer, and in turn, the bubbles become stable. After achieving stability of the bubbles, additional AEA dosage is required (part 2) for generating enough bubbles to cover the entire container surface and achieve foam index. The additional AEA dosage required to generate enough bubbles to cover the entire surface should depend on the cross-sectional area of the bottle. This mechanism supports the observation made in Harris et al. (2008a, 2008b, 2008c), who showed that changes in fill ratio and dimension of the foam index container affects the foam index test result.

To further understand the effect of AEA type and LOI of the ash on the evolution of empty area fraction, the dosage required to make the foam layer stable (part 1) and the dosage required to achieve complete coverage of the test container surface (foam index) were plotted (Figure 6). In general, the foam index increased with LOI content (Figure 6-A). The foam index was higher for the vinsol resin-based AEA compared to the sodium olefin sulfonate-based AEA. However, the AEA dosage required to achieve stable foam was higher for the sodium olefin sulfonate-based AEA compared to the vinsol resin-based AEA. The ratio of foam index and part 1 did not change much with different LOI values but was different for the two different AEAs tested. Part 1 is related to the adsorption of AEA onto the fly ash particles and, thus, is expected to depend both on the AEA and the fly ash characteristics. The second part depends on the surface tension of the solution, and mostly depends on the AEA type, as well as container geometry. Thus, part 1 of this digital foam index test provides additional insights regarding the fly ash AEA interaction mechanisms and can potentially be a better indicator of AEA dosage requirement for concrete mixes.



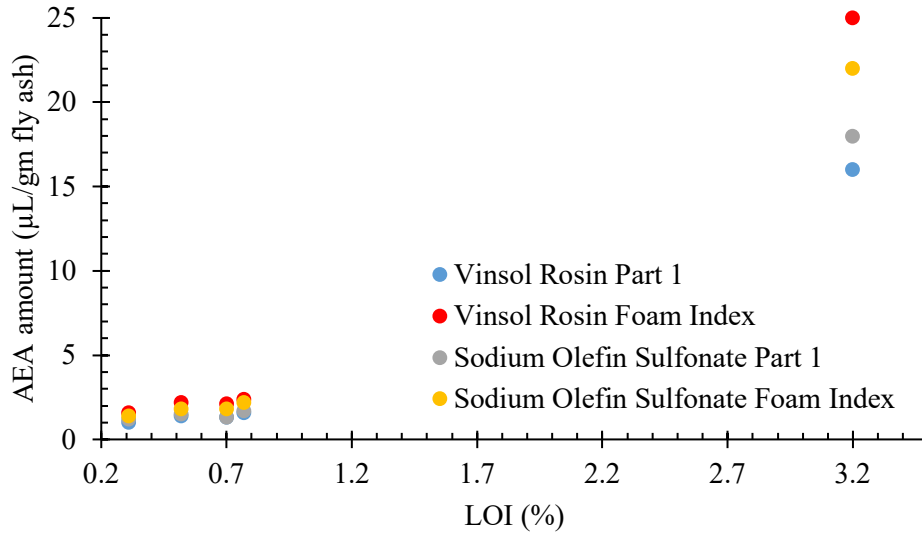
A. Different AEA dosage additions for a representative fly ash sample (fly ash 3)



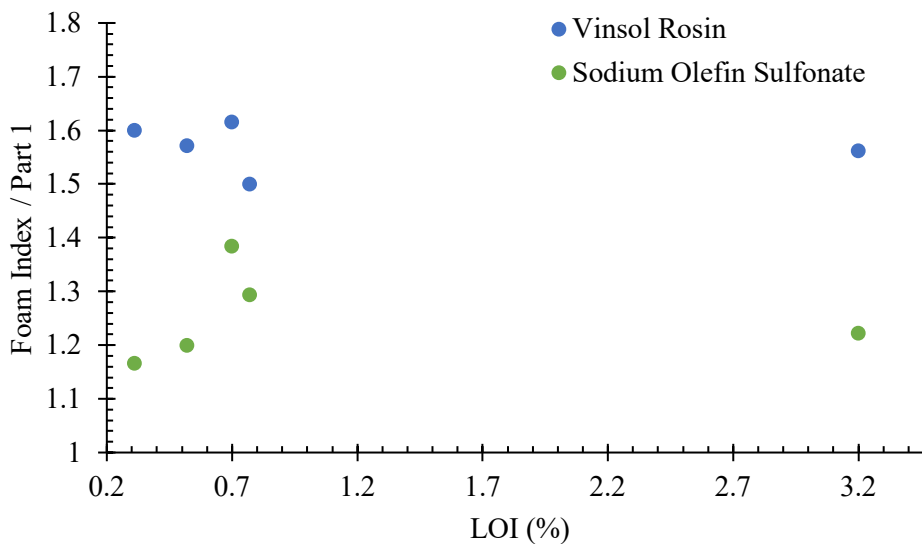
B. Fraction of empty areas with number of drops of AEA

**Figure 5. Graphs. Change in empty area fraction with time (a) for different AEA dosage additions for a representative fly ash sample (fly ash 3). The evolution of empty area with number of drops of AEA addition for different times after stopping the shaking is shown in (b). Both figures use the same digital foam index test data.**

*Source: Baral, Roesler, and Fu (2021)*



A. AEA dosage required for making the foam layer stable and the foam index for different ashes with different LOIs



B. Ratio of foam index and AEA dosage required for making the foam layer stable

**Figure 6. Graphs. AEA dosage required for making the foam layer stable and the foam index for different ashes with different LOIs (a). The ratio of foam index and AEA dosage required for making the foam layer stable is plotted in (b).**

*Source: Baral, Roesler, and Fu (2021)*

## SETTING TIME

The initial and final setting times of concrete are very important for efficient construction of concrete pavement, as curing, tining, and saw cutting are dependent on setting times. Moreover, a very long setting time can cause plastic shrinkage cracks, as the amount of plastic shrinkage is directly

proportional to the final setting time (Gołaszewski et al. 2017). There are multiple methods to measure setting times such as the vicat needle test (ASTM C191 2019), ultrasound wave propagation (Öztürk et al. 2006; Reinhardt, Große, and Herb 2000), calorimetry (Hu, Ge, and Wang 2014), and noncontact ultrasound (Tran and Roesler 2020, 2021). Calorimetry is one of the most convenient lab methods to estimate hydration, heat flow, and setting time.

Isothermal calorimetry can also be used to predict the trends in the initial and final setting times. As shown in Figure 7, the initial inflection point of the heat flow curve (second derivative set to zero) has been defined as the initial setting time, whereas peak 1, the  $C_3S$  hydration peak, has been previously defined as the final setting time (Hu, Ge, and Wang 2014). The lower amount of gypsum present in the under-sulfated system lowers the amount of  $Ca^{2+}$  dissolving from gypsum, which in turn decreases the C-S-H precipitation rate and delays the  $C_3S$  peak hydration time. Thus, moderately under-sulfated systems have a longer final setting time compared to a well-sulfated system. However, a significant deficiency in sulfates in the HVFAC can potentially lead to flash setting and a very short set time (Beckemeier 2012). The setting times obtained from calorimeter data should not directly compare with the setting times obtained from ASTM C403 (2016) penetration tests, but the trends in setting time among different mixes observed from calorimeter data is similar to the trend observed from the standard ASTM tests (Hu, Ge, and Wang 2014). A calorimeter can be used quickly and conveniently to evaluate setting times of different mix designs, sources of cement and fly ash, chemical admixture, and limestone replacement.

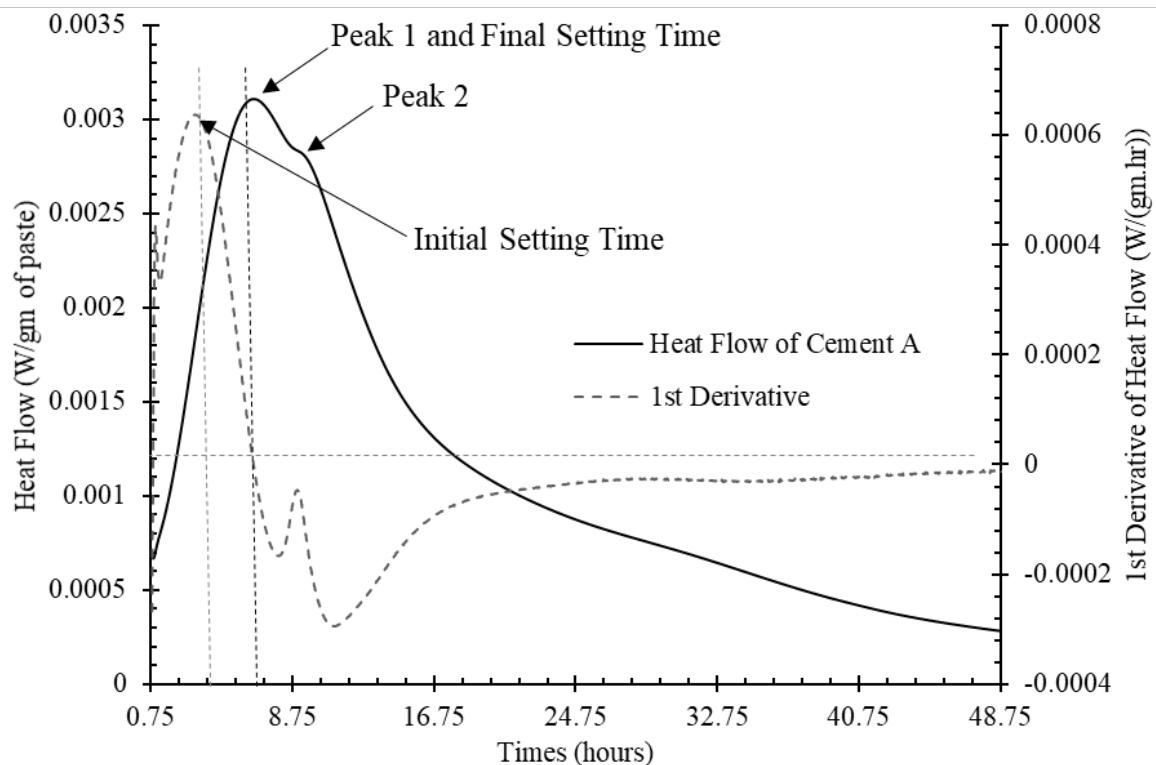


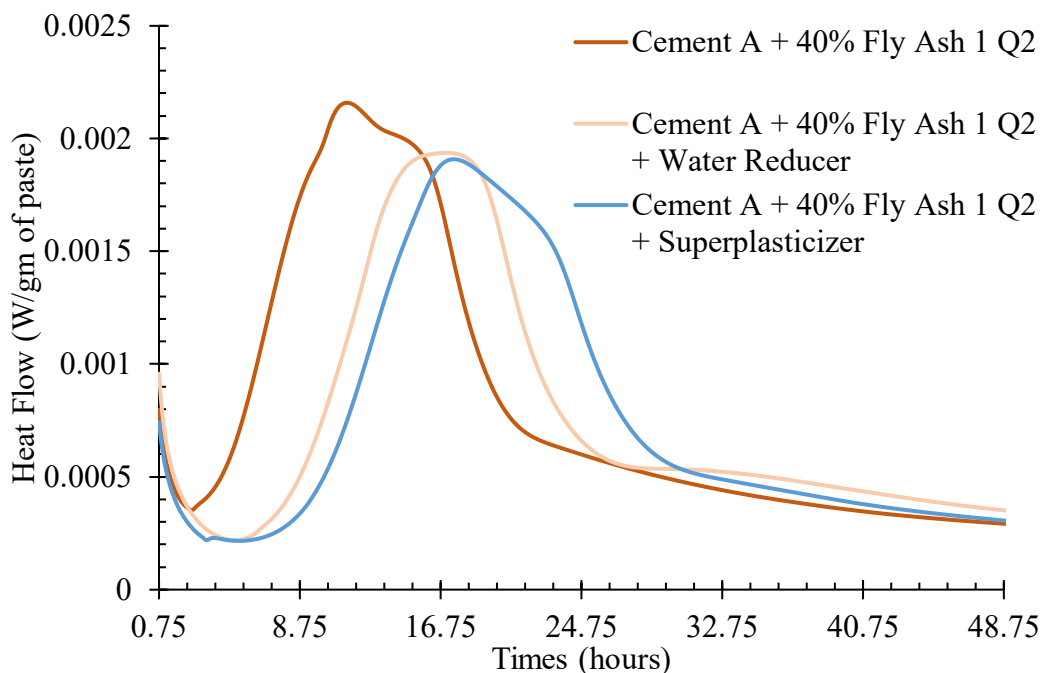
**Figure 7. Graph. Isothermal calorimetry results for a sample Portland cement with initial and final setting times of 3.3 hours and 6.5 hours, respectively.**

**Source: Baral, Roesler, and Fu (2021)**

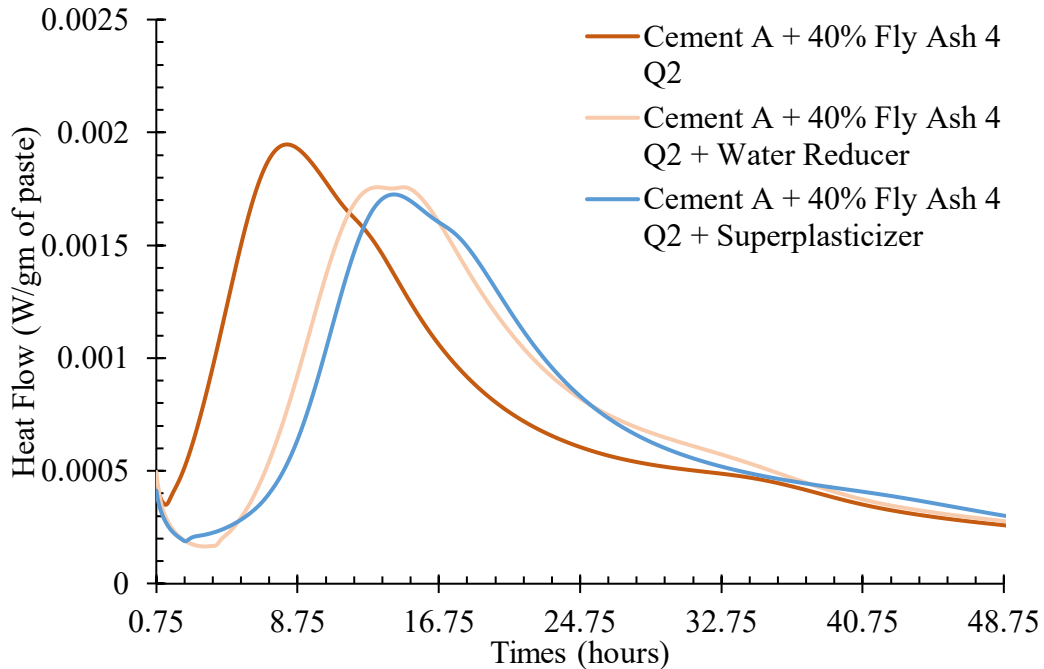
## Effect of Chemical Admixtures on Setting Time

Chemical admixtures are used in concrete to provide workability as well as accelerate or retard the hydration reaction. In this report, the effect of a water reducer and a superplasticizer that improve the workability of HVFAC mixes was studied. The middle point of the dosage recommended by the manufacturer (300 mL/100 kg (4.6 oz/100 lb) binder for both the superplasticizer and water reducer) was used for the calorimeter tests. The superplasticizer was polycarboxylate ether (PCE) based, whereas the water reducer was lignosulfonate based. PCE- and lignosulfonate-based admixtures provide workability using two different mechanisms. The lignosulfonate salt dissolves in water and releases a cation, making the admixture molecule negatively charged. The negatively charged lignosulfonate gets attached to cement particles through electrostatic force and makes all the cement particles negatively charged and thus minimize flocculation. In contrast, PCE-based admixture molecules have a large negatively charged backbone with shorted sidechains. The PCE backbone is adsorbed on the cement grains (especially on the aluminate phases as they are positively charged), and the sidechains stop the flocculation through steric hindrance. As steric hindrance is the major factor providing workability, PCE-based admixtures are not affected by the change in ion concentration over time and thus provides workability for a longer time compared to the lignosulfonate-based admixtures.

Both the water reducer and superplasticizer delayed the hydration reaction significantly. The induction period was consistently longer for the PCE-based admixture compared to the lignosulfonate one (Figure 8), which also led to a further delay in setting times (Table 1). The setting times were delayed by 4–5 hours and 5–6 hours for the water-reducer and superplasticizer usage, respectively.



A. Fly Ash 1 (Class C)



B. Fly Ash 4 (Class F)

**Figure 8. Graphs. Effect of superplasticizer and water reducer on heat flow rates for 40% weight replacement of cement with (a) Fly Ash 1 (Class C), (b) Fly Ash 4 (Class F) for 2019 quarter 2 samples.**

*Source: Baral, Roesler, and Fu (2021)*

**Table 1. Effect of Chemical Admixtures on Setting Times of HVFAC (Cement A + 40% Fly Ash)**

		Initial Setting Time (hr)	Final Setting Time (hr)
<b>Fly Ash 1</b>	Control	7.0	11.0
	Water Reducer	12.4	15.1
	Superplasticizer	13.0	17.0
<b>Fly Ash 4</b>	Control	4.7	8.2
	Water Reducer	9.7	13.1
	Superplasticizer	10.6	14.0

### Set Time Acceleration with Limestone

Limestone is the main raw material in cement production and is directly used as coarse aggregates in concrete. Even though limestone is generally considered an inert material, it can react with the aluminate phases and form monocarbonate and hemicarbonates. The addition of limestone powder (micro and nano) to accelerate the setting times have been investigated. Nanomaterials offer a very high specific surface area and provide nucleation sites for calcium silicate hydrate precipitation. Thus, nano-limestone is expected to affect the hydration reaction rate of HVFAC more than the addition of micro-limestone (Bentz 2011). In this work, the average particle size of the nano-limestone used was within 15–40 nm, whereas the micro-limestone particles were smaller than 50 microns.

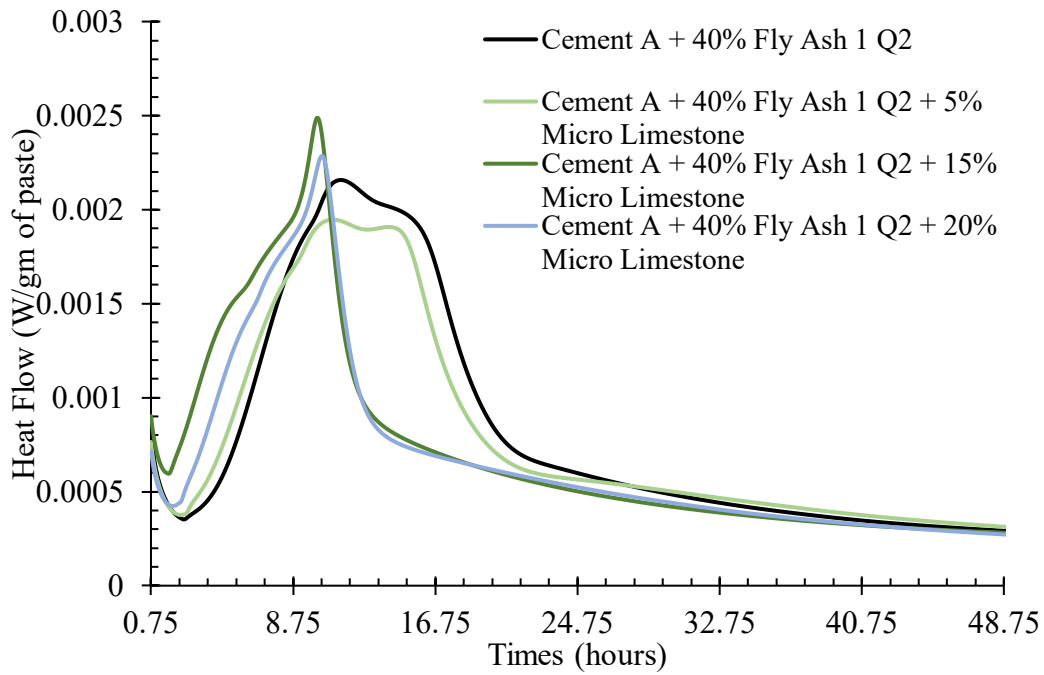


### HVFA Mixes without Chemical Admixtures: Effect of Limestone Particle Size

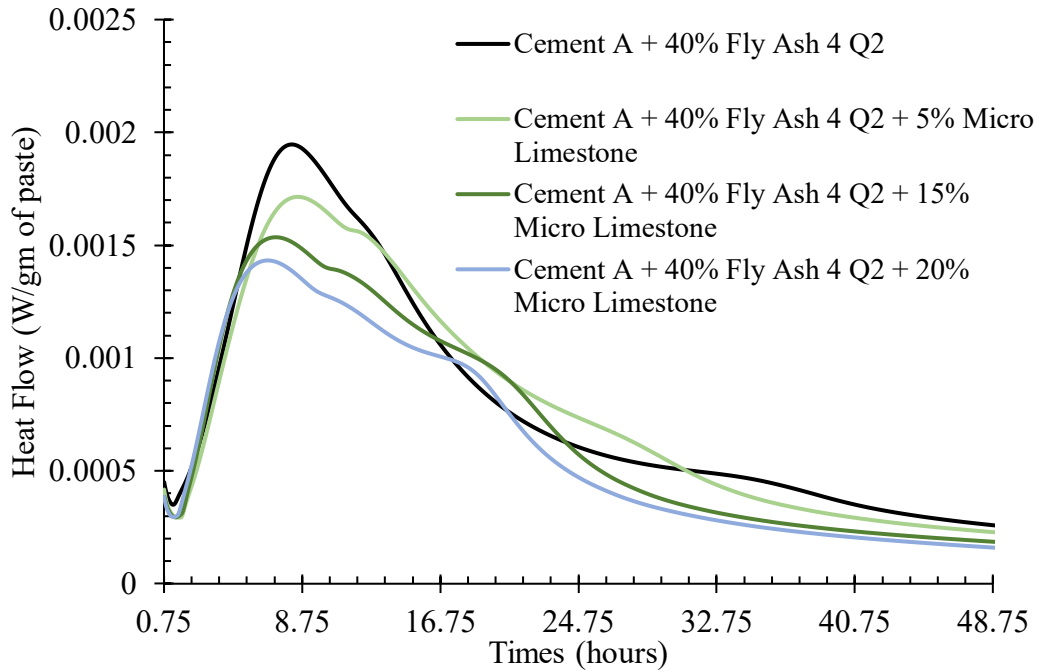
For HVFA mixes, nano-limestone replacement was more effective in accelerating the setting times compared to micro-limestone. Increasing nano-limestone addition to 10% for Fly Ash 1 decreased the initial and final setting time by 3.2 and 2.7 hours, respectively (Figure 9 and Figure 10). The set time acceleration was slightly lower for the system with 40% Fly Ash 4 (Class F) and 10% nano-limestone, as initial and final setting times were 2.3 and 2.5 hours faster, respectively (Table 2). Thus, limestone replacement was able to accelerate setting time, and calorimeter was able characterize this acceleration in set times.

### Effect of Chemical Admixtures on HVFA with Micro-limestone

A 5% replacement of micro-limestone was used to evaluate its effect on accelerating the retardation caused by chemical admixture addition. Similar to the HVFA mixes without any limestone, the PCE-based superplasticizer increased the induction period longer than the lignosulfonate-based water reducer for the HVFA mixes with 5% micro-limestone (Figure 11). Thus, the superplasticizer mixes had longer setting times than the water-reducer ones (Table 3). Even though the different chemical admixtures had a retarding effect, even on HVFA mixes with 5% micro-limestone, the micro-limestone replacement had a significant effect on accelerating the setting times by 2–3 hours compared to HVFA mixes with chemical admixtures (Table 4). For Class F mixes (Fly Ash 4), the setting time acceleration due to 5% micro-limestone replacement was similar for mixes with PCE- and lignosulfonate-based admixtures. However, for Class C mixes, the acceleration was much higher in PCE-based admixture mixes compared to the lignosulfonate-based mix. Thus, micro-limestone replacement at a low amount can be a great tool to accelerate the setting times without sacrificing long-term strength. Moreover, micro-limestone is already widely available in the United States and can be applied to high-volume, ready-mix concrete mixes.



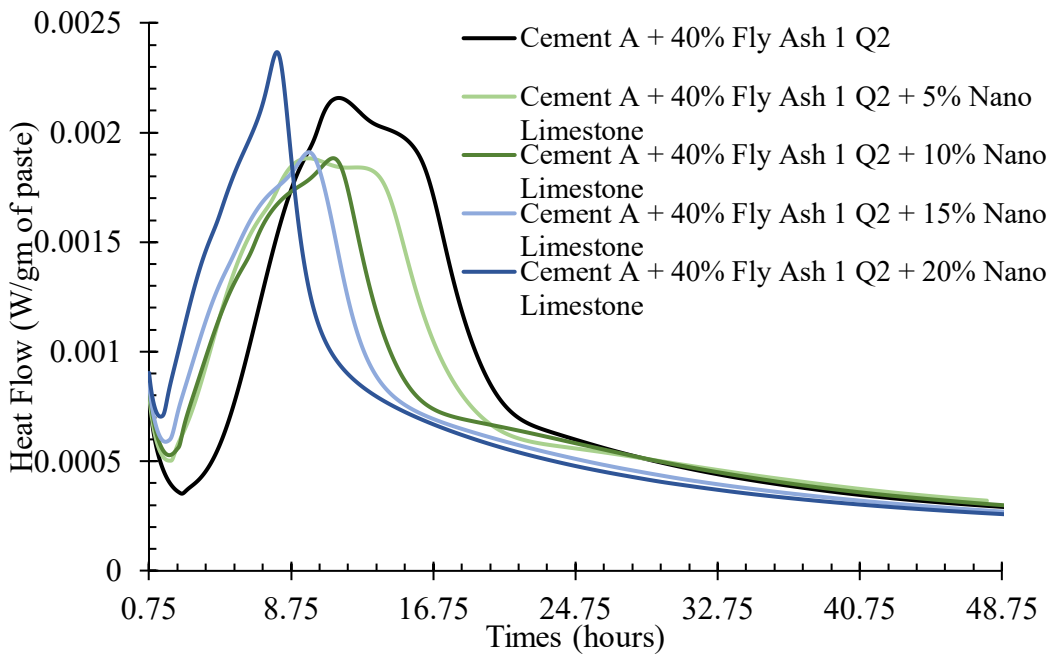
A. Fly Ash 1 (Class C)



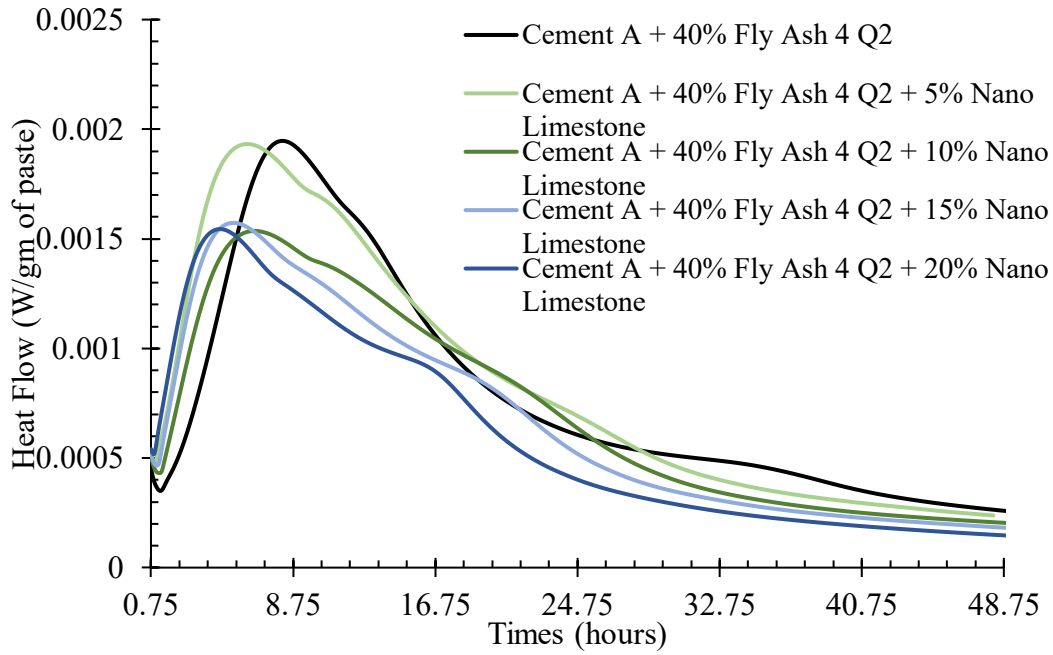
B. Fly Ash 4 (Class F)

Figure 9. Graphs. Effect of increasing micro-limestone replacement on heat flow rates for 40% weight replacement of cement with (a) Fly Ash 1 (Class C), (b) Fly Ash 4 (Class F) for 2019 quarter 2 samples.

Source: Baral, Roesler, and Fu (2021)



A. Fly Ash 1 (Class C)



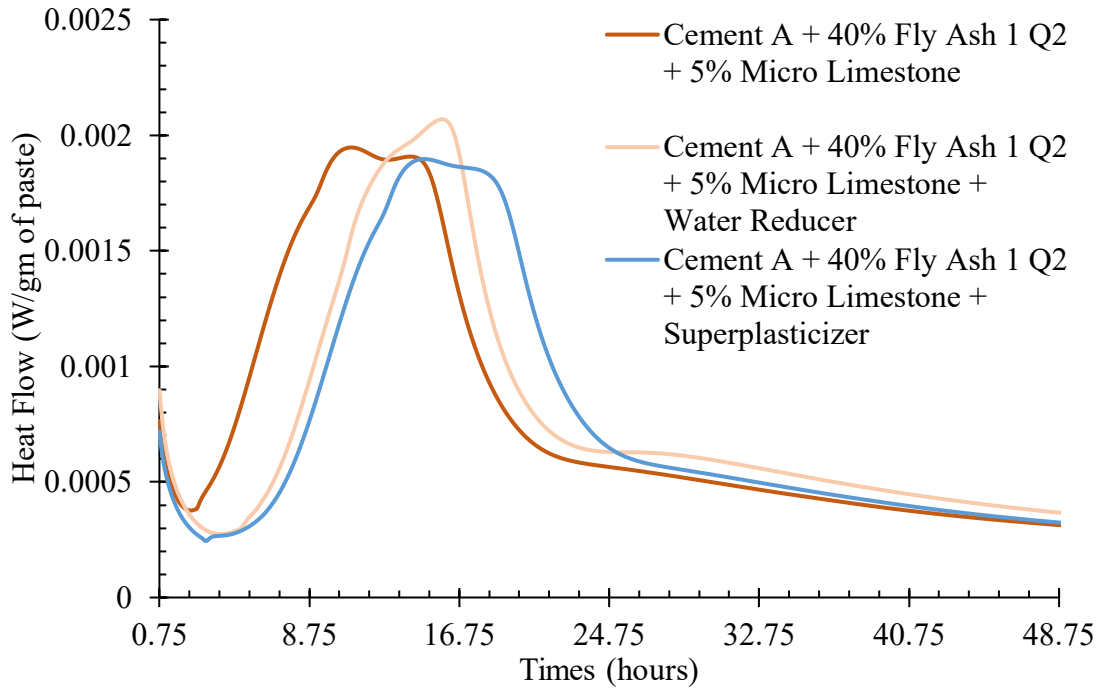
B. Fly Ash 4 (Class F)

Figure 10. Graphs. Effect of increasing nano-limestone replacement on heat flow rates for 40% weight replacement of cement with (a) Fly Ash 1 (Class C), (b) Fly Ash 4 (Class F) for 2019 quarter 2 samples.

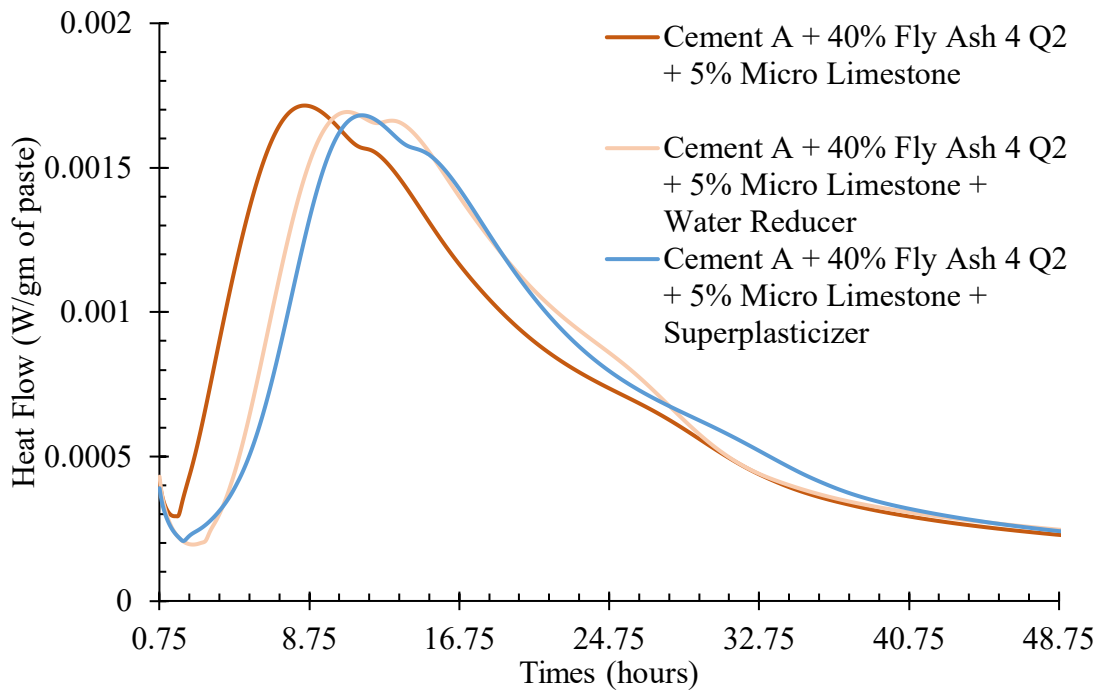
Source: Baral, Roesler, and Fu (2021)

Table 2. Effect of Limestone Replacement of Cement on Setting Time of HVFA Mixes

		Micro-limestone		Nano-limestone	
		Initial Setting Time (hr)	Final Setting Time (hr)	Initial Setting Time (hr)	Final Setting Time (hr)
Fly Ash 1	0%	7.0	11.0	7.0	11.0
	5%	5.8	9.3	4.2	9.0
	10%	–	–	3.7	8.3
	15%	3.3	6.0	2.2	7.6
	20%	4.3	6.5	1.8	5.9
Fly Ash 4	0%	4.7	8.2	4.7	8.2
	5%	3.7	8.4	2.4	6.1
	10%	–	–	2.3	5.9
	15%	3.3	7.2	1.3	5.2
	20%	3.0	6.7	1.1	4.7



A. Fly Ash 1 (Class C)



B. Fly Ash 4 (Class F)

**Figure 11. Graphs. Effect of superplasticizer and water reducer on heat flow rates for 5% micro-limestone and 40% weight replacement of cement with (a) Fly Ash 1 (Class C), (b) Fly Ash 4 (Class F) for 2019 quarter 2 samples.**

**Source: Baral, Roesler, and Fu (2021)**

**Table 3. Effect of Superplasticizer and Water Reducer on Setting Times for 5% Micro-limestone and 40% Weight Replacement of Cement with Different Fly Ash Sources**

		Initial Setting Time (hr)	Final Setting Time (hr)
Fly Ash 1	Control	5.8	9.3
	Water Reducer	10.9	13.2
	Superplasticizer	9.6	14.2
Fly Ash 4	Control	3.7	8.4
	Water Reducer	6.5	10.2
	Superplasticizer	7.9	11.4

**Table 4. Effect of 5% Micro-limestone Replacement on the Acceleration of Setting Times**

		Acceleration in Initial Setting Time (hr)	Acceleration in Final Setting Time (hr)
Fly Ash 1	Control	1.2	1.7
	Water Reducer	1.5	1.9
	Superplasticizer	3.4	2.8
Fly Ash 4	Control	1	-0.2
	Water Reducer	3.2	2.9
	Superplasticizer	2.7	2.6

### Noncontact Ultrasound Device for Setting Time Measurement

The setting time of concrete is related to the penetration resistance of the concrete. According to ASTM C403 (2016), penetration resistance of 500 and 4,000 psi is related to the initial and final setting times of concrete, respectively. The penetration resistance of concrete indicates the development of compressive, tensile, and shear resistance of the hydrating paste. In its plastic state, concrete has little to no shear resistance, but as concrete hydrates, significant shear resistance develops with time (Figure 12). Thus, tracking the shear resistance of concrete directly or indirectly can potentially indicate the setting time of concrete. One of the ways to indirectly track shear resistance development is the propagation of leaky Rayleigh waves. The noncontact ultrasound setting time measurement device developed by Tran and Roesler (2021) measures the energy of the leaky Rayleigh wave transmission and can be used to determine the final setting time both in the field and laboratory.

This device uses an electrostatic-type ultrasonic transducer to transmit a 16-cycle 50 kHz ultrasonic pulse and three MEMS sensors as receivers. An acoustic baffle is placed in between the transmitter and receivers to reduce the direct-air acoustic signal. The receiver signal is then processed to calculate the leaky Rayleigh wave energy received over time. A sudden sharp increase of the leaky-Rayleigh wave energy is taken as the final setting time. A detailed description of the test method and calculations can be found in Tran and Roesler (2021). A detailed schematic of the test setup is shown in Figure 13.

This device was used to determine the final setting time of concrete in the field pavement test section. Two HVFAC mixes were also prepared: one with a chemical admixture and one without a

chemical admixture to verify its applicability on the HVFAC mix. The setting times obtained from the calorimeter and noncontact ultrasound devices were comparable, in general (Table 5). Note that the calorimeter test was performed at 22°C (71.6°F), and the noncontact ultrasound test was performed at 25°C (77°F).

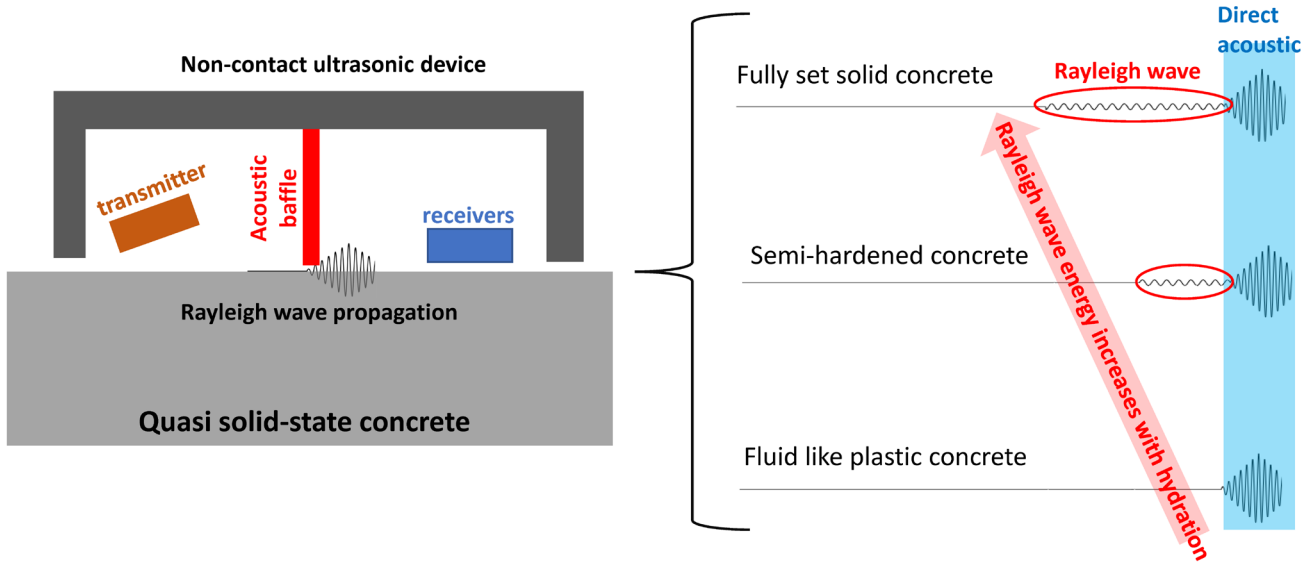


Figure 12. Schematic. Leaky Rayleigh wave propagation in concrete at different stages of hydration.

Source: Baral, Roesler, and Fu (2021)

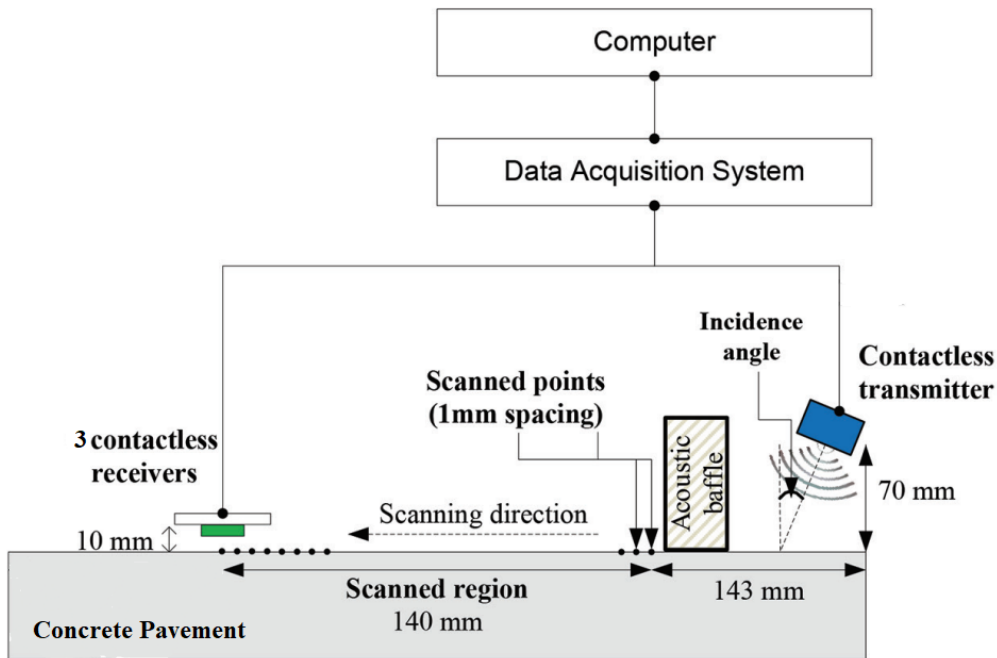


Figure 13. Schematic. Noncontact ultrasound setting time measurement device.

Source: Modified from Tran and Roesler (2021)

**Table 5. Final Setting Time Comparison between Noncontact Ultrasound Device and Isothermal Calorimeter**

Mix Name	Calorimeter	Noncontact Ultrasound
40% FA mix, with water reducer and AEA	13 hours	12 hours
40% FA mix, no chemical admixtures	10 hours	8 hours

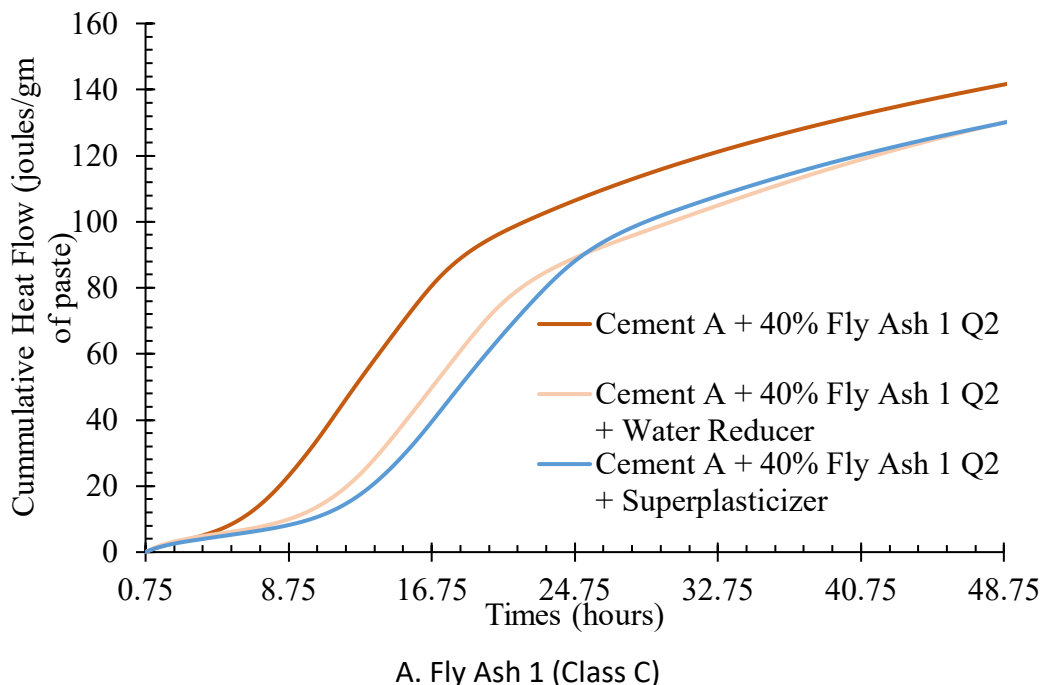
## STRENGTH

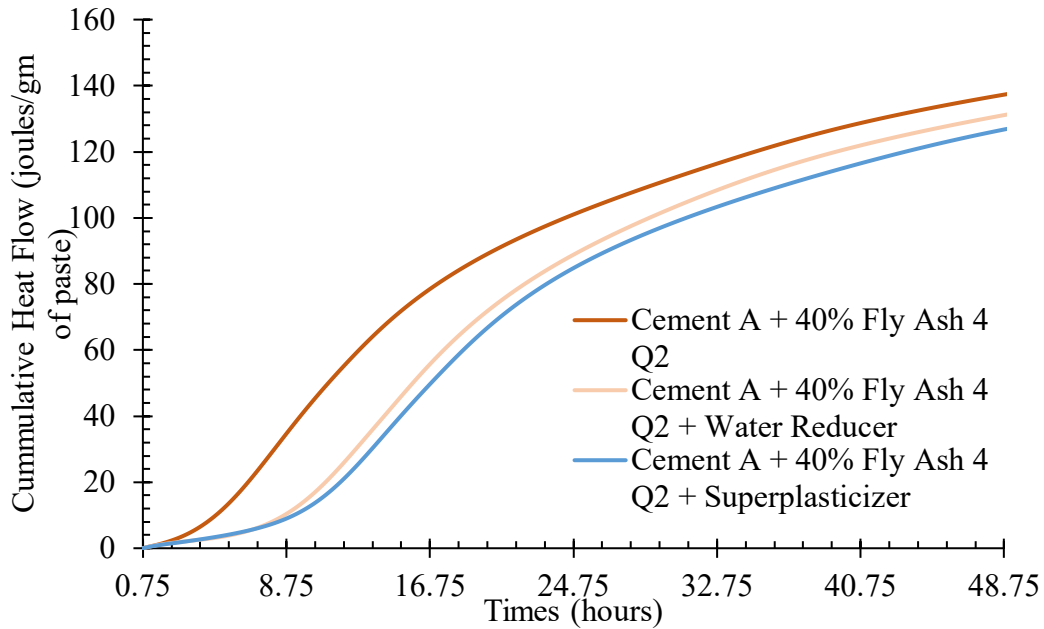
Compressive strength gain of HVFAC is slower than conventional concrete, and, thus, it needs to be monitored. Two ways of measuring early-age strength can be used: (1) 48-hour cumulative heat flow in the calorimeter test and (2) 3-day concrete cylinder results. The first method is a quick and simple way to test potential strength gain issues of many mixes. It can also be used to quantify the effect of chemical admixture additions on the hydration of HVFAC. However, the cumulative heat flow should not be compared directly with compressive strength given that the calorimeter test only evaluates the hydration reaction, whereas compressive strength is a combination of aggregate packing, paste-aggregate bond, and the hydration reactions.

## Calorimeter Tests

### *Effect of Chemical Admixtures on 48-hour Cumulative Heat Release*

The cumulative heat release after 48 hours was similar for both lignosulfonate- and PCE-based admixtures, and they were about 5%–15% less than the control mix without any chemical admixtures for both Class C and F fly ash (Figure 14).





B. Fly Ash 4 (Class F)

**Figure 14. Graphs. Effect of superplasticizer and water reducer on cumulative heat flow for 40% weight replacement of cement with (a) Fly Ash 1 (Class C), (b) Fly Ash 4 (Class F) for 2019 quarter 2 samples.**

*Source: Baral, Roesler, and Fu (2021)*

#### *Hydration Acceleration with Limestone Replacement*

For HVFA mixes with no chemical admixtures, the cumulative heat released after 48 hours decreased with increasing limestone replacement. For some types of fly ash, the cumulative heat release after 48 hours increased when 5% of the cement was replaced with nano-limestone, but for micro-limestone replacement, the cumulative heat released after 48 hours was always lower than the control mix. For HVFA mixes with PCE-based superplasticizer or lignosulfonate-based water reducer, a 5% micro-limestone placement had only about 5% lower heat after 48 hours compared to mixes without any micro-limestone replacement.

### **Concrete Strength Test**

#### *Mixture Design*

For the strength testing, a conventional concrete with 100% cement was compared to 20% fly ash and 40% fly ash replacement with the 19 different fly ash sources. These mixture designs used the three main mixture constituents and proportions shown in Table 6. No air-entraining or water-reducing admixtures were used in this strength testing.



**Table 6. Mixture Designs**

Mixture	w/b	Cement (kg [lb])	Fly Ash (kg [lb])	Water (kg [lb])	Paste (%)	Coarse (kg [lb])	Fine (kg [lb])
OPC	0.45	283 (625)	0 (0)	127 (281)	28.8	863 (1903)	564 (1243)
20% fly ash	0.45	227 (500)	57 (125)	127 (281)	28.9	862 (1900)	562 (1240)
40% fly ash	0.45	170 (375)	113 (250)	127 (281)	29.0	858 (1892)	557 (1228)

**Slump Test**

Slump tests were performed for each mixture following ASTM C143 to characterize the various mixtures' workability. Figure 15 displays the slumps for all fly ash, comparing the 20% to 40% mixtures and the control ordinary Portland cement (OPC) mix.

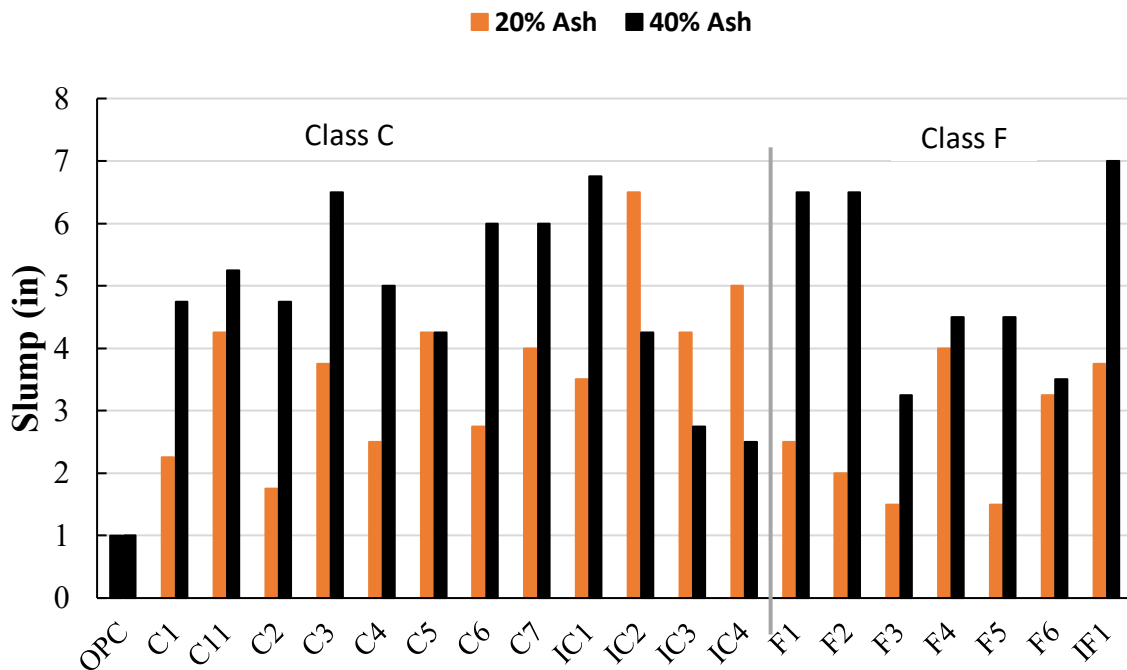


**Figure 15. Graph. Comparison of slumps measured for each fly ash mixture at 20% and 40% replacement levels with the control (OPC).**

*Source: Ley et al. (2021)*

In most cases, the 40% mixtures had a higher slump than the mixtures at 20% replacement by an average of 3.05 cm (1.2 in.). Of the Class C mixtures, C6 and IC1 showed the greatest increase in slump at 8.26 cm (3.25 in.). Of the Class F mixtures, F2 fly ash showed the greatest increase in slump with 2 in. at 20% compared to a slump of 16.5 cm (6.5 in.) at 40% replacement. However, this is not always the case. IC2, IC3, and IC4 showed higher slumps at the 20% replacement compared to 40% by 5.72 cm (2.25 in.), 3.81 cm (1.5 in.), and 6.35 cm (2.5 in.), respectively, while F6 and F4 showed little effect on the slumps for the 40% mixture. C5 had no change in slumps between 20% and 40% replacement levels. These differences in slumps are likely caused by differences in the particle size

distribution or gradation of the fly ash and the cement and how they interact. This is an area of future study.

**Compressive Strength Testing of Samples at 3 Days and 90 Days**

Figure 16 shows all the 20% fly ash mixtures as a percent of OPC at 3 and 90 days. OPC of 100% is denoted by a solid black horizontal line. Standard deviations are indicated by lines above and below each data point, except for cases with deviations less than 1%. Class C and F fly ash are divided by the vertical grey line. Class C fly ash in general reached the strength of the control at 3 days, the minimum being C4 and IC1 at 91% and C5 reaching the greatest at 135%. No Class F fly ash reached the strength of OPC at 3 days, which is typical of the pozzolanic behavior of Class F fly ash. However, they did reach within 20% of OPC, with IF1 reaching 83% and F2 reaching 95%.

All mixtures met or exceeded the strength of OPC at 90 days by as much as 135%, except F4. The maximum for Class C, C5 reached 135% at 90 days, while F1, F2, and F3 fly ash reached a maximum of 121% of OPC at 90 days.

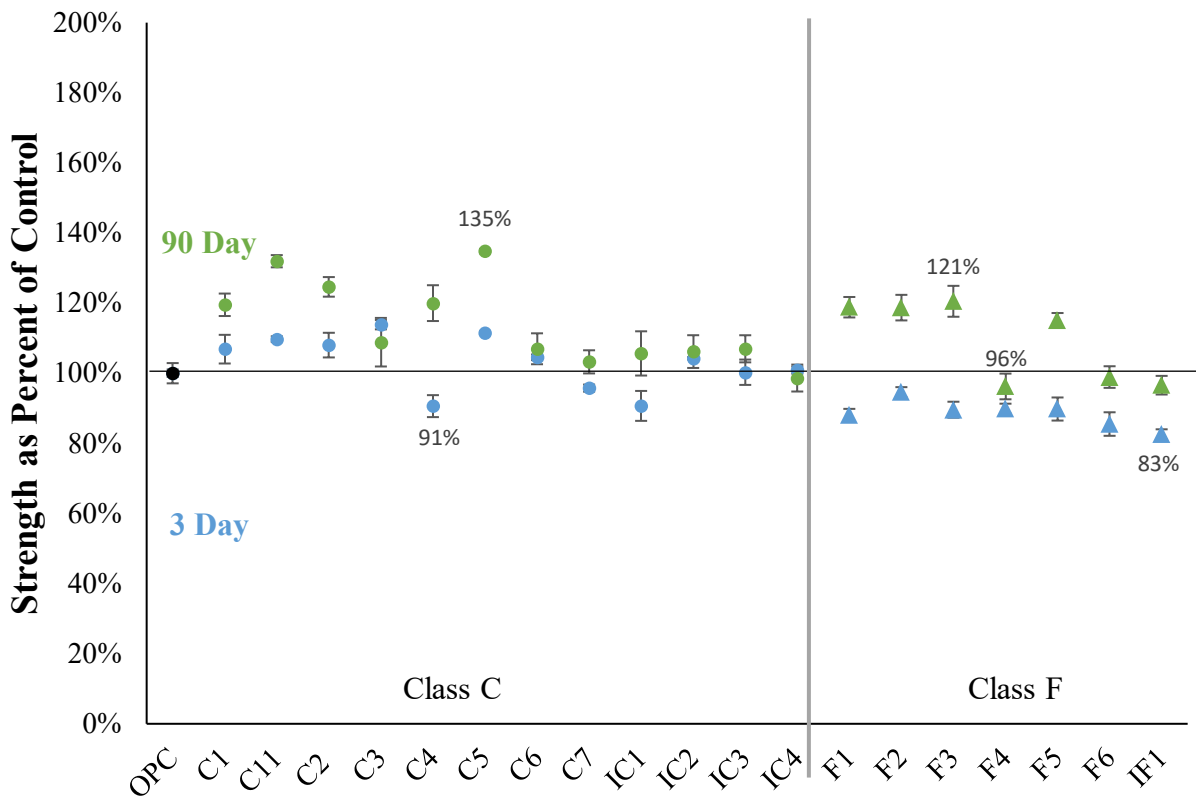


**Figure 16. Graph. 20% fly ash mixtures compressive strength as a percent of the control at 3 and 90 days of hydration.**

**Source: Ley et al. (2021)**

Figure 17 shows all 40% fly ash mixtures as a percent of OPC at 3 and 90 days with OPC of 100% denoted by the solid black horizontal line. One standard deviation is shown by the lines above and

below each data point, except for cases with deviations less than 1%. Class F fly ash did not show as much reactivity compared to Class C at three days with 40% replacement. This is most likely attributed to the pozzolanic effect of Class F fly ash, which requires more time due to the delayed reactions and is magnified by the amount of replacement. IF1 only reached 51% of OPC at three days, the maximum being F2 at 80% of OPC. C6 had the lowest overall strength for Class C at three days with 59%; the rest of the Class C fly ash were within 35% of OPC. Fly ash F4 reached the greatest strength for the Class F fly ash with 120% of OPC at 90 days; the minimum was IF1 at 87%. Class C fly ash all met or exceeded OPC at 90 days, except for C6, which reached 89%. The highest was C4 at 126%, though C3 was right behind at 125%.

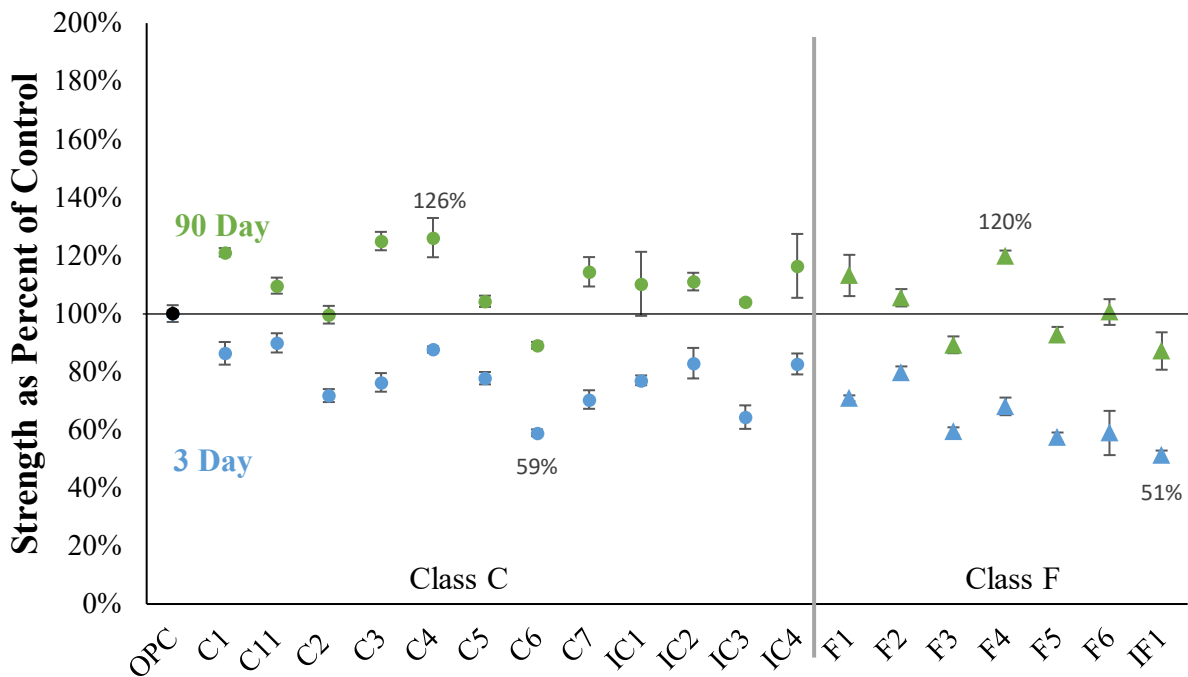


**Figure 17. Graph. 40% fly ash mixtures compressive strength as a percent of the control at 3 and 90 days of hydration.**

**Source: Ley et al. (2021)**

Data in Figure 17 indicate that mixtures with 40% fly ash replacement may not reach the strength of OPC at 3 days. However, they do meet and often exceed the strength of OPC at 90 days. Some fly ashes are performing better than others because of a combination of their particle size distribution and reactivity level.

# CHAPTER 3: PARTICLE MODEL FOR HVFAC STRENGTH DEVELOPMENT AND DURABILITY

The particle model was developed based on the assumption that the elemental composition of fly ash particles can be an indication of the major phase in that particular group. This assumption is supported by previous research showing that the fly ash particles are primarily composed of a single dominant phase mixed with minor phases (Hu, Aboustait, et al. 2014; Hu, Ley, et al. 2014; Kutcho and Kim 2006). This is based on using an Automated Scanning Electron Microscope (ASEM) to classify thousands of individual fly ash particles (Aboustait et al. 2016; Chen et al. 2004; Ghosal, Ebert, and Self 1995; Kim, Moradian, and Ley 2018; Kim et al. 2018; Kim et al. 2020) and then machine learning. The self-organizing map algorithm was applied to classify the fly ash particles into nine distinct groups based on these few major repeatable patterns of chemical compositions (Kim et al. 2018). These nine group compositions were used to derive predictive models over different concrete properties at varying hydration times for different fly ash replacement levels. The percentage of each group was used to conduct a multivariable linear regression analysis to construct the linear model for predicting the performance of cement-based materials, including fly ash.

The outline of the particle model is presented in Figure 18. The particle model has demonstrated a promising ability to predict the compressive strength, electrical resistivity, and apparent diffusion coefficient of concrete with 20% and 40% fly ash replacement rates at different hydration times. Furthermore, this particle model provides an important opportunity to study the variance of the elemental compositions of individual particles and their effectiveness in a concrete mixture, which helps users better characterize different fly ash sources and determine applicability of a source for higher volume fly ash concrete.

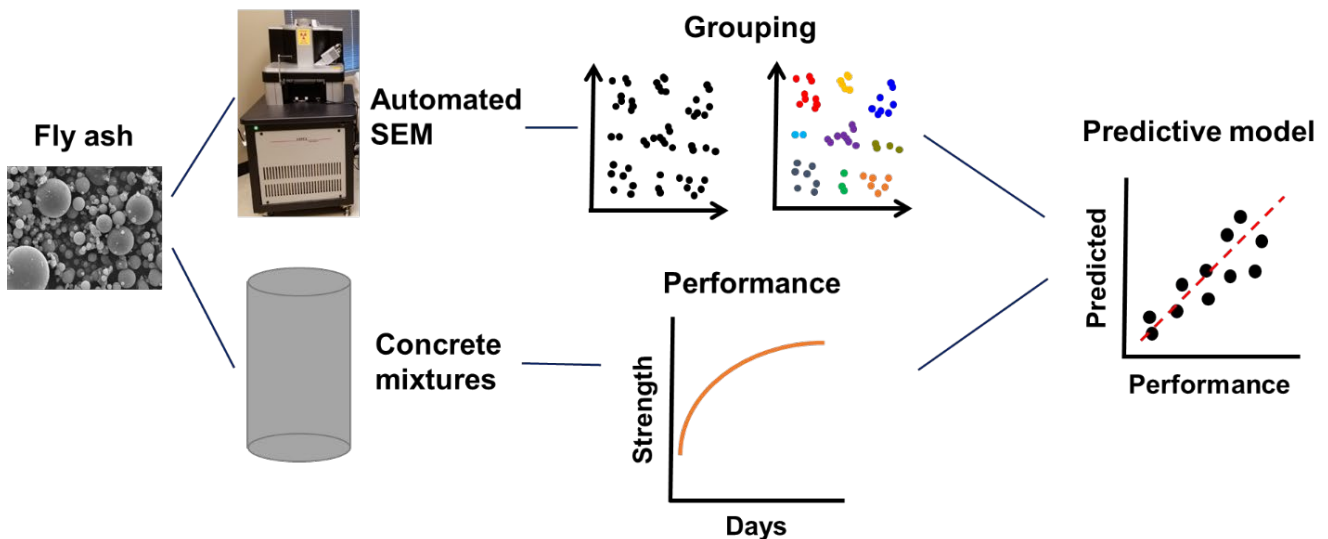


Figure 18. Photo. The comprehensive procedure of the particle model.

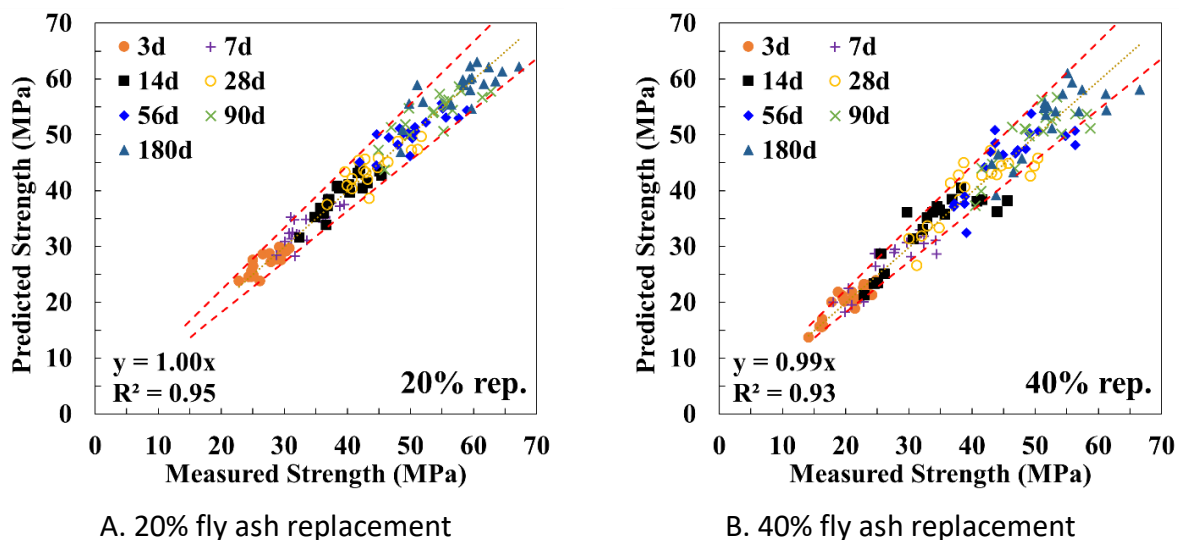
Source: Kang, Ley, et al. ( 2020)

## PARTICLE MODEL TO PREDICT COMPRESSIVE STRENGTH

Figure 19 demonstrates the relationship between the measured and predicted values using the particle model for all curing times for concrete with 20% and 40% fly ash replacement of cement. Twelve Class C and seven Class F fly ash sources were used for these concrete mixtures. The fly ash sources were chosen based on a range of different chemical compositions. A constant 0.45 water-to-cementitious material ratio (w/cm) was used for all mixtures. No chemical admixtures were added to these mixtures to minimize the variables.

The slope of the trend line for 20% and 40% replacement are 1.00 and 0.99, respectively, and the R-squared value of each trend line for 20% and 40% replacement are 0.95 and 0.93, respectively. This shows the compressive strength is accurately predicted by using the particle model for each curing time (age).

According to ASTM C39, the acceptable range of three individual cylinder strengths for the test of 100 by 200 mm (4 by 8 in.) cylinders made from a well-mixed sample of concrete under laboratory conditions is 10.6%. This is a helpful number to evaluate the accuracy of the particle model. Values of  $\pm 10\%$  are shown in Figure 19 as red dashed lines. For the 20% fly ash replacement shown in Figure 19-A, 127 out of 133 measurements, or 95% of all measurements, are within  $\pm 10\%$ , and the remaining six predictions are within  $\pm 15\%$ . For the concrete with 40% fly ash replacement in Figure 19-B, 108 out of 133, or 81% of the measurements, are within  $\pm 10\%$  and 94% of the predictions are within  $\pm 15\%$ . This indicates that the particle model works well, and the derived equations are reliable to predict the compressive strength from periods between 3 days and 180 days with both 20% and 40% replacement. Thus, the particle model can be considered as a robust tool to predict the compressive strength of fly ash concrete for the materials investigated. More information can be found in other publications (Kang, Lloyd, et al. 2020; Kang, Ley, and Behravan 2021).



\* Red dashed line: The range of  $\pm 10\%$  of the predicted and measured strength.

**Figure 19. Graphs. Relationship between the predicted and measured strength by using the particle model for (a) 20% fly ash concrete and (b) 40% fly ash concrete for ages 3 to 180 days.**

*Source: Kang, Lloyd, et al. (2020)*

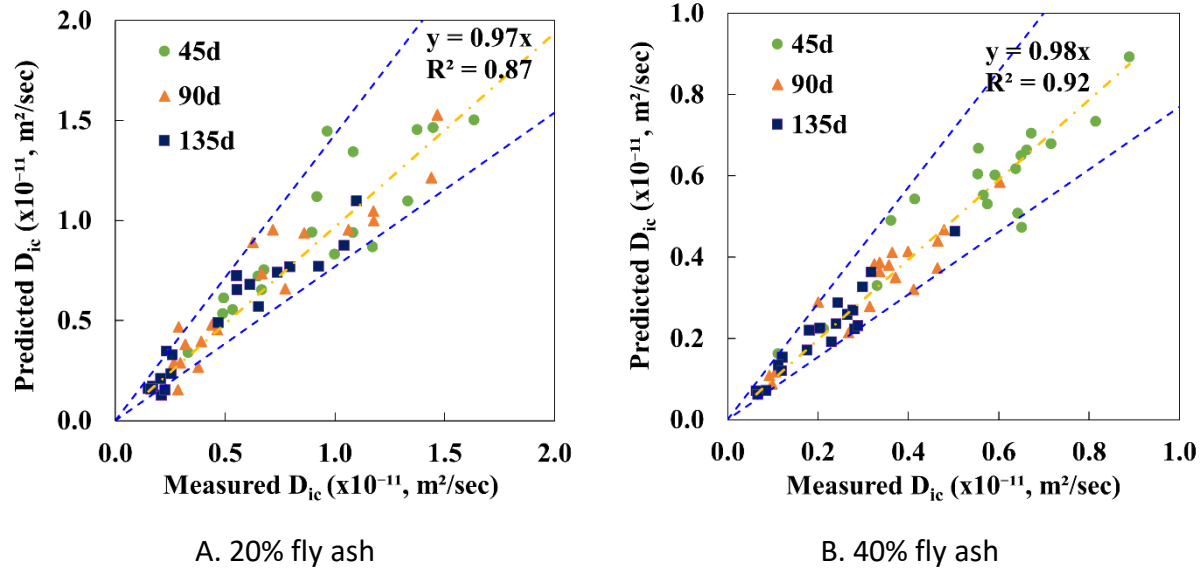
## PARTICLE MODEL TO PREDICT DIFFUSION COEFFICIENT

The diffusion test used 19 types of fly ash (the same as the compressive strength test). The paste mixtures have a 0.45 water-to-cement ratio (w/cm) at a 20% and 40% fly ash replacement rate by mass of cement. All mixtures were prepared as per ASTM C305. Vials with dimensions of 9.5 mm × 46 mm (0.375 in. × 1.811 in.) were used to prepare the paste samples, and then the samples were sealed and cured at 23°C (73.4°F) until day 45, 90, or 135. Three samples were prepared for each curing time for each fly ash mixture.

The comparisons between the predicted apparent iodide diffusion coefficient ( $D_{ic}$ ) from the particle model and measured  $D_{ic}$  is described in Figure 20. The slope of the trend line of the 20% fly ash replacement rate is 0.97 and that of the 40% fly ash replacement rate is 0.98. The R-squared value of each trend line for 20% and 40% replacement is 0.87 and 0.92, respectively. This shows the  $D_{ic}$  is quite accurately predicted by using the particle model for each curing time (age).

While there is no reported variability of the Transmission X-ray Microscopy (TXM) and detection of iodide that is used to determine the  $D_{ic}$  in this testing, the variation of other tests that measure the same property is widely reported in the literature. For example, Tang (2008) evaluated the precision of the diffusion coefficient through various methods such as the immersion test (Nordtest method NT build 492), rapid migration test (Nordtest method NT build 443), and measurement of chloride ion ingress test (EN 13396). The study suggests the coefficient of variation (CV) of these tests are 24%, 28%, and 36%, respectively. The average CV is 29.3% or close to 30%. Moreover, ASTM C1556 (bulk chloride diffusion test) provides 39.8% as the limit of CV to evaluate the precision (single laboratory) of determining the apparent  $D_{ic}$  of cementitious mixtures. Because these tests measure the diffusion of ions, a value of  $\pm 30\%$  is assumed to be a good estimate of the  $D_{ic}$  for this testing and is shown by a blue dashed line in Figure 20.

The data in Figure 20 shows that 86% and 95% of comparisons are within  $\pm 30\%$  for 20% and 40% fly ash, respectively. Moreover, the regression of the trend line shows as  $y = 0.97x$  for 20% fly ash and  $y = 0.98x$  for 40% fly ash. Furthermore, the R-squared value of the regression is quite similar to 0.87 and 0.92 for 20% and 40%, respectively. This means there is no difference in the variability of the  $D_{ic}$  between 20% and the 40% fly ash samples. The predictions of the particle model can repeatedly predict the  $D_{ic}$  of 20% and 40% replacement level of fly ash in cement paste. More information can be found in other publications (Kang, Ley, and Behravan 2021; Kim et al. 2020).



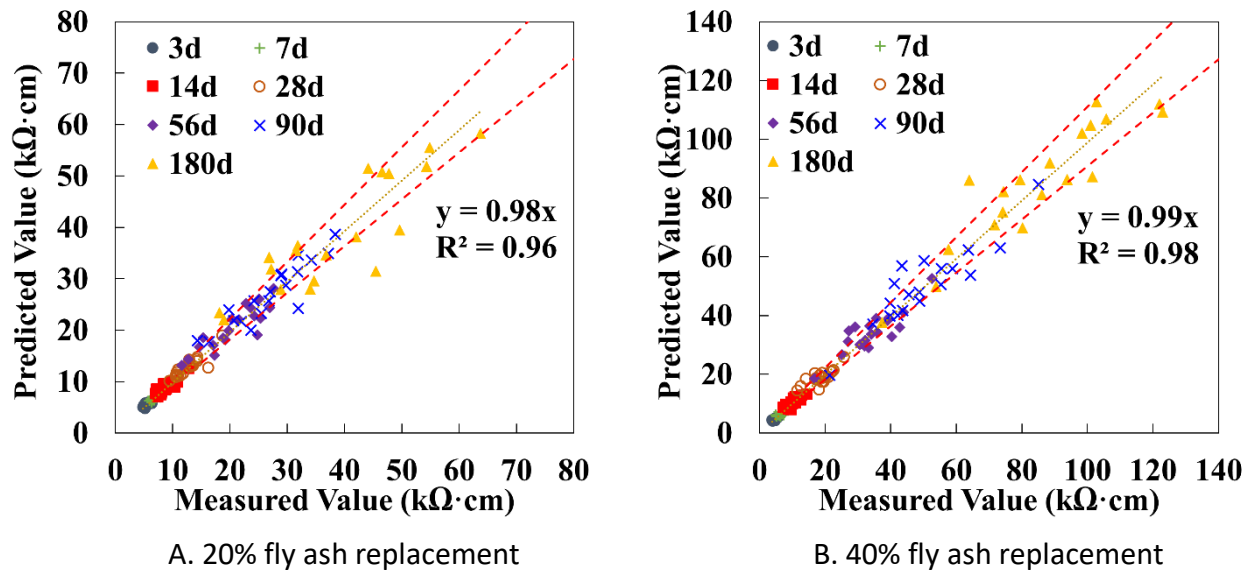
\* Blue dashed line: The range of +/- 30% of the calculated and measured properties.

**Figure 20. Graphs. Comparison between the calculated and measured values for  $D_{ic}$ .**

*Source: Kang, Ley, and Behravan (2021)*

## PARTICLE MODEL TO PREDICT RESISTIVITY FOR HVFAC

A nondestructive surface resistivity test, the four-point Wenner probe, was used to measure the electrical resistivity of the concrete following AASHTO T 358. The comparisons between the calculated resistivity value with the predictive models by using the particle model and measured resistivity value are shown in Figure 21-A for 20% and Figure 21-B for 40% fly ash replacement. The slope of the trend line in the comparisons for both 20% and 40% fly ash replacement are at the level of 0.96 and 0.99, respectively. This suggests the results are a very good fit. In addition, the accuracy of the calculated value using the particle model is evaluated with the +/- 10% red dashed lines. Of the predictions, 107 out of 133 are within +/- 10%, while 14 predictions are added with the limit of +/- 15% and the remaining 12 predictions are out of +/- 15% for 20% fly ash replacement, as shown in Figure 21-A. In the case of 40% fly ash replacement in Figure 21-B, 98 out of 133, or 75% of the measurements, show a difference within a range of +/- 10%, while 10 predictions are added with the limit of +/- 15%, and the remaining 25 predictions are out of +/- 15%. While there is some variability, overall, the resistivity is accurately predicted with the help of the particle model. Thus, the particle model can be considered as a robust tool to predict the electrical resistivity of fly ash concrete for the materials investigated. More information can be found in other publications (Kang, Ley, et al. 2020; Kang, Ley, and Behravan 2021).



\* Red dashed line: The range of +/- 10% of the predicted and measured resistivity.

**Figure 21. Graphs. Comprehensive relationship between the calculated and experimental resistivity for (a) 20% fly ash replacement and (b) 40% fly ash replacement.**

*Source: Kang, Ley, et al. (2020)*

## COMPARING RESISTIVITY AND DIFFUSION COEFFICIENT

The Nernst-Einstein equation in Figure 22 is used to investigate the correlation between electrical resistivity ( $\rho_{sr}$ ) and the apparent iodide diffusion coefficient ( $D_{ic}$ ). This approach has been widely used because the test method for electrical resistivity is quick, easy, and nondestructive, and it helps to avoid time-consuming grinding of the samples (Andrade, d'Andrea, and Rebolledo 2014; Ryan et al. 2014; Liu, Presuel-Moreno, and Paredes 2015; Xiao et al. 2016). A value for K was calculated by using all data sets at 20% and 40% fly ash replacement. The R-squared value for each derived equation was investigated as well as the number of data points that are located within +/- 30% of the predicted  $D_{ic}$  value because this is a reasonable range for the measurement of this test method. The Nernst-Einstein equation is:

$$D_{ic} = K/\rho_{sr}$$

**Figure 22. Equation. Nernst-Einstein equation.**

where,  $D_{ic}$  is the apparent iodide diffusion coefficient [ $\times 10^{-11}$ ,  $m^2/s$ ];  $\rho_{sr}$  is the surface electrical resistivity of the concrete sample [ $k\Omega \cdot cm$ ]; K is a factor that shows the correlation between  $D_{ic}$  and  $\rho_{sr}$ . The value of K in Figure 22 can be varied, depending on the test method for determining the  $D_{ic}$ , the type of fly ash, and the fly ash replacement level (Liu, Presuel-Moreno, and Paredes 2015).

The accuracy was examined by developing a predictive equation and then determining the percentage of data correctly predicted to be within the variation of the apparent diffusion coefficient test methods or +/- 30% of the predicted value. Figure 23 presents a comparison between the  $\rho_{sr}$  and



$D_{ic}$  for 20% and 40% replacement levels of fly ash. These plots treat all fly ash the same and do not separate them by Class C or F. The measurement of the mixture with just OPC is also shown in each figure. A total of 57 comparisons between  $\rho_{sr}$  and  $D_{ic}$  are made for each fly ash replacement level and three comparisons with OPC. The mixtures with OPC show almost no changes in  $D_{ic}$  or  $\rho_{sr}$  between day 45 and day 135. However, the samples with 20% fly ash show that 35% of the  $D_{ic}$  are higher than the  $D_{ic}$  of OPC at day 135 and only one of the samples with 40% fly ash replacement has a higher  $D_{ic}$  than OPC. Moreover, for both fly ash replacement levels, once the  $\rho_{sr} > 25 \text{ k}\Omega\cdot\text{cm}$ , then the  $D_{ic}$  values are less than the lowest value for OPC at day 135 ( $0.8 \times 10^{-11} \text{ m}^2/\text{s}$ ). This is true for 96% of the samples for 20% fly ash and 100% of the samples for 40% fly ash. This indicates that the relationship between  $\rho_{sr}$  and  $D_{ic}$  is different for OPC and 20% or 40% fly ash. Also, a constant  $\rho_{sr}$  value can determine if a concrete mixture with 20% or 40% fly ash replacement can improve the  $D_{ic}$  value over the  $D_{ic}$  of OPC for the materials and mixtures investigated.

The fitting coefficient  $K$  is found to be 17.02 for 20% fly ash and 14.84 for 40% fly ash. Each equation using the calculated  $K$  value is described with the black curve in Figure 23. A value of  $\pm 30\%$  has been added in Figure 23 as the pink dashed line as an estimate for the variability of the  $D_{ic}$ . For 20% fly ash, the result shows that only 58% of the comparisons are within  $\pm 30\%$ . In other words, just more than half of the  $D_{ic}$  of 20% fly ash concrete can be estimated by using  $\rho_{sr}$ , within the expected variation of the test method, if a single  $K$  value is used. For 40% fly ash, 81% of the comparisons are within  $\pm 30\%$  limitation. This indicates that  $\rho_{sr}$  shows a good prediction of the  $D_{ic}$  for 40% fly ash replacement, but it could be improved for 20% fly ash replacement.

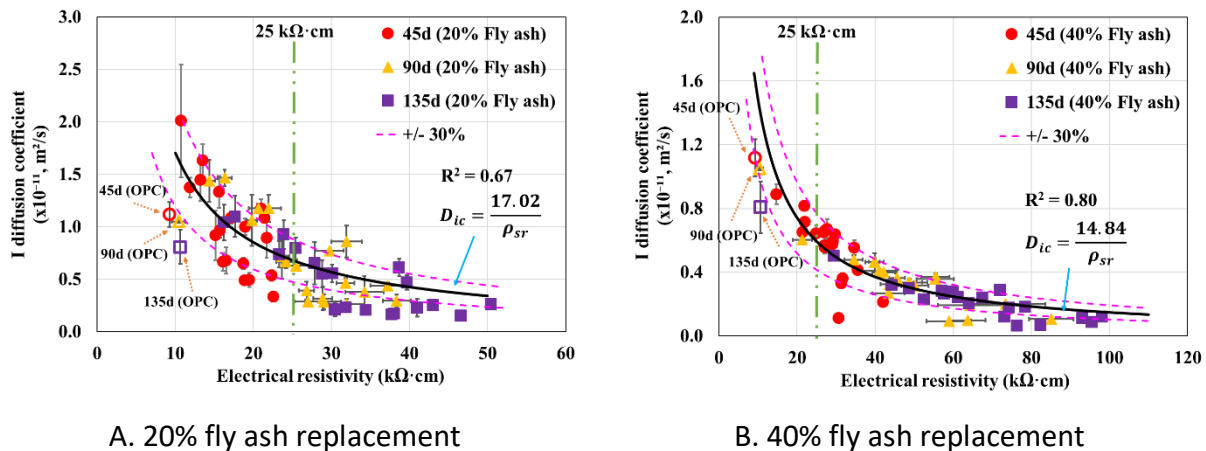


**Figure 23. Graphs. Comprehensive correlation between  $\rho_{sr}$  and  $D_{ic}$  for samples with fly ash and OPC.**

*Source: Kang et al. (2021)*

To try and improve the agreement between  $\rho_{sr}$  and  $D_{ic}$ , the fly ash was separated by Class C and F at 20% and 40% fly ash replacement, respectively. Overall, the Class F fly ash exhibit a higher  $\rho_{sr}$  and lower  $D_{ic}$  than that of Class C fly ash for both 20% and 40% fly ash replacement. The results from the regression analysis and the number of points within the expected variation of the test are summarized in Table 7.

**Table 7. Summary of K and R-squared Values for All Investigations**

Fly ash Data use	20%			40%		
	All	Class C	Class F	All	Class C	Class F
K value (95% CI*)	17.02 (15.62, 18.41)	18.68 (17.15, 20.21)	11.13 (10.11, 13.55)	14.84 (13.94, 15.74)	15.35 (14.23, 16.47)	13.36 (11.91, 14.82)
R-squared	0.67	0.70	0.62	0.80	0.77	0.82
Percentage within +/- 30%	58%	75%	67%	81%	92%	71%
<b><u>K<sub>s</sub></u></b>	<b><u>22</u></b>	<b><u>24</u></b>	<b><u>16</u></b>	<b><u>19</u></b>	<b><u>20</u></b>	<b><u>17</u></b>
<b><u>Percentage within + 30%</u></b>	<b><u>86%</u></b>	<b><u>92%</u></b>	<b><u>86%</u></b>	<b><u>96%</u></b>	<b><u>100%</u></b>	<b><u>90%</u></b>

\*CI: confidence interval

By separating the mixtures by Class C and F fly ash, the accuracy of the prediction for 20% fly ash replacement was 75% for Class C fly ash and 67% for Class F fly ash. For 40% fly ash replacement, the accuracy of the prediction was 92% for Class C fly ash and 71% for Class F fly ash.

These findings suggest the relationship between  $\rho_{sr}$  and  $D_{ic}$  is more influenced by the type of fly ash at 20% fly ash replacement than 40% fly ash. Further, the R-squared values are much improved at 40% fly ash samples than 20% fly ash samples. This means that a single regression equation to predict the  $\rho_{sr}$  and  $D_{ic}$  relationship shows more promise at higher fly ash replacement levels than lower levels, and therefore, the accuracy of using the Nernst-Einstein equation is affected by not only the fly ash replacement rate, but also the type of fly ash. This difference might be caused by the different types of reactions that occur in Class C fly ash compared to Class F fly ash, and this may cause a change in the pore solution chemistry and the subsequent  $\rho_{sr}$  measurements while not impacting the  $D_{ic}$ . The formation factor aims to reduce this and is an area of future study.

Even though there is not a single K value that can be used to predict the performance of 20% or 40% fly ash replacement using +/- 30% limits, there is a method to use  $\rho_{sr}$  to conservatively estimate  $D_{ic}$  with this work. This method uses the upper limit or the +30% line of the relationship in Figure 23 as a conservative estimate for  $\rho_{sr}$  and  $D_{ic}$ . The K value used for the +30% line is known as  $K_s$ . A plot of all 20% fly ash replacements is shown in Figure 24-A with a +30% line and  $K_s$ , and the 40% fly ash replacement is shown in Figure 24-B with a +30% line and  $K_s$ . Furthermore, the derived  $K_s$  and the percentage of samples that have a  $D_{ic}$  that is at or below this value are shown in Table 7. The results show that different  $K_s$  are determined with only Class C fly ash data or Class F fly ash data. This allows a specification to be created by choosing the desired service life of the structure and then finding the  $D_{ic}$  that would provide this. Next,  $D_{ic}$  is divided by  $K_s$  to determine the required  $\rho_{sr}$  for the specification. This allows a practitioner to specify a  $\rho_{sr}$  value and have a high level of confidence ( $\approx$  95% confidence level) that the correct  $D_{ic}$ , and therefore the service life, value will be obtained in the concrete.

For example, an owner may choose a  $D_{ic}$  of  $0.75 \times 10^{-11} \text{ m}^2/\text{s}$  to obtain a 50-year service life. This means that a  $\rho_{sr}$  value of 30  $\text{k}\Omega\text{-cm}$  should be specified for a 20% fly ash mixture and a value of 25  $\text{k}\Omega\text{-cm}$  should be specified for a 40% fly ash mixture. These values are shown in Figure 24-A and Figure 24-B, respectively. The replacement levels between these values could be linearly interpolated. Trial batches can be tested with surface resistivity at different days, and once the  $\rho_{sr}$  exceeds this value, then the mixture can be accepted as providing the desired  $D_{ic}$ . More information can be found in other publications (Kang et al. 2021).

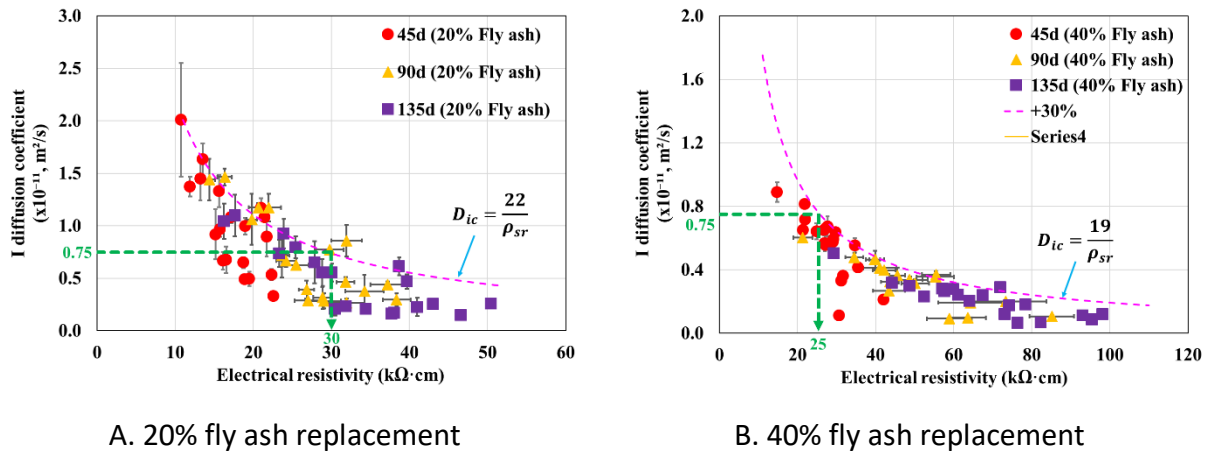


**Figure 24. Graphs. All comparisons for 20% and 40% fly ash replacement with +30% limit line and  $K_s$ . Lines are also included to show an example of using the  $K_s$  relationship.**

*Source: Kang et al. (2021)*

## RECOMMENDATIONS FOR ASR / SALT SCALING / FREEZE-THAW BASED ON THE LITERATURE REVIEW

Fly ash is an invaluable tool for improving the durability of concrete. For example, fly ash is the primary method to reduce the alkali-silica reaction (ASR). The AASHTO R 80 document provides sound guidelines to use fly ash to suppress ASR. As previously discussed, the carbon in fly ash can impact the ability to entrain air in concrete, and this can impact the freeze-thaw durability. This document shows that the foam index test can be used as a performance test to evaluate fly ash–AEA interactions and can determine its dosage in concrete. This provides more benefit over using LOI to evaluate fly ash–AEA interactions. There has been concern that high volumes of fly ash can cause salt-scaling issues. Recent research shows that scaling is more of an issue with hand-finished concretes, such as sidewalks. For surfaces that are primarily machine finished, like a pavement, salt-scaling is not an issue in the field. Based on this work, the American Concrete Institute (ACI) is in the process of changing its requirements in ACI 201—Concrete Durability.

## CHAPTER 4: FIELD IMPLEMENTATION OF HVFAC

Successful implementation of HVFAC in the field will require monitoring the air content, workability, setting time, and concrete opening strength to traffic (construction and public). The workability of HVFA concrete pavement can be monitored with the traditional slump cone test and its target value will depend on whether the HVFAC casting be side formed, slip formed, or hand placed. Air content will also need to be monitored to maintain a durable concrete to resist freeze-thaw cycles with the pressure air meter (6% air content) and Super Air Meter (SAM) number (0.2).

The setting time of the HVFAC will control the time of multiple construction activities (curing, texturing, saw cutting). The setting time can be estimated by monitoring the internal temperature of the concrete pavement or other indirect means such as the noncontact ultrasonic method. The following sections will cover concrete opening strength through maturity monitoring and setting time characterization with noncontact ultrasound.

### FIELD MATURITY METHOD FOR STRENGTH

Based on the field test sections in Canton, Illinois, and complementary lab testing, the maturity method can successfully indicate the compressive strength of the in situ HVFAC pavement. Figure 25 provides a layout for measuring temperature (via wireless thermal sensors) with depth (1.3 cm [0.5 in.], 7.6 cm [3 in.], 19 cm [7.5 in.], and 22.9 cm [9 in.] from the surface of the concrete) to provide the data for calculating the maturity of the HVFAC. The control pavement section had a similar length, width, joint details, and sensor layout.

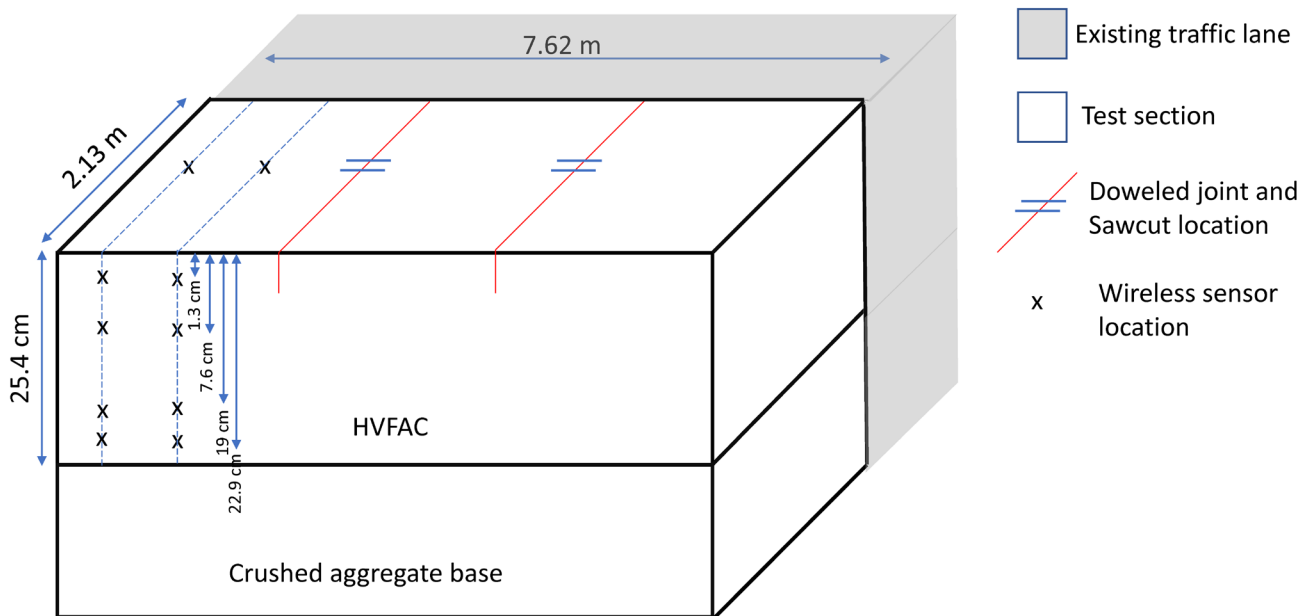


Figure 25. Photo. HVFAC field pavement test section details (not to scale).

Source: Baral, Roesler, and Fu (2021)

In the lab or during a trial batch in the field, a maturity calibration curve must be constructed relating the compressive strength over time to maturity of the HVFAC. An example of a strength versus age for a HVFAC and control concrete (20% fly ash) is shown in Figure 26 for two patching mixes. (See Table 8 for mixture designs.) As expected in Figure 26 the strength gain of the HVFAC mix was significantly lower than the control mix, but the 28-day strength for both the mixes was equal—49 MPa (7100 psi) (Figure 26). Current IDOT policy requires Class PV concrete to achieve 24 MPa (3,500 psi) compressive strength in 14 days, whereas concrete patching mixtures (Class PP-1) must have 22 MPa (3,200 psi) strength within 48 hours. Both mixes used in this project were PP-1 mix and thus required to reach 22 MPa (3,200 psi) compressive strength in 48 hours.

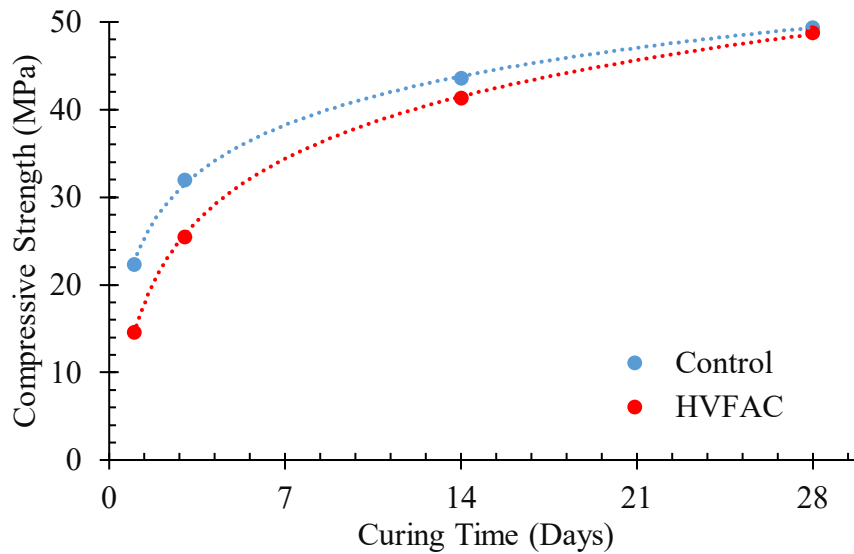


Figure 26. Graph. Compressive strength vs. age for control and HVFA concrete mixes.

Source: Baral, Roesler, and Fu (2021)

Table 8. Mix Design and Fresh Properties of Control and HVFA Concrete Mixes

	Unit	Control Mix	HVFAC
<b>Cement</b>	Kg/m <sup>3</sup> (lbs/yd <sup>3</sup> )	304 (512)	247 (416)
<b>Fly Ash</b>	Kg/m <sup>3</sup> (lbs/yd <sup>3</sup> )	103 (174)	162 (273)
<b>Coarse Aggregate</b>	Kg/m <sup>3</sup> (lbs/yd <sup>3</sup> )	1080 (1821)	1082 (1824)
<b>Fine Aggregate</b>	Kg/m <sup>3</sup> (lbs/yd <sup>3</sup> )	700 (1179)	705 (1189)
<b>Water</b>	L/m <sup>3</sup> (gal/yd <sup>3</sup> )	129 (26)	119 (24)
<b>Air Entrainer</b>	mL/m <sup>3</sup> (oz/yd <sup>3</sup> )	232 (6)	309 (8)
<b>Water Reducer</b>	mL/m <sup>3</sup> (oz/yd <sup>3</sup> )	812 (21)	812 (21)
<b>Superplasticizer</b>	mL/m <sup>3</sup> (oz/yd <sup>3</sup> )	696 (18)	696 (18)
<b>Air Content</b>	%	5.7	5.1
<b>Air Content from SAM</b>	%	5.8	5.5
<b>SAM No</b>		0.3	0.1
<b>Slump</b>	cm (in.)	(6.25)	(5.5)

The maturity calibration curve is constructed next from the measured temperatures in the cast cylinders. The temperature-time factor is calculated using the Nurse-Saul equation. The maturity calibration curve is shown in Figure 27 for the two mixtures in Table 8.

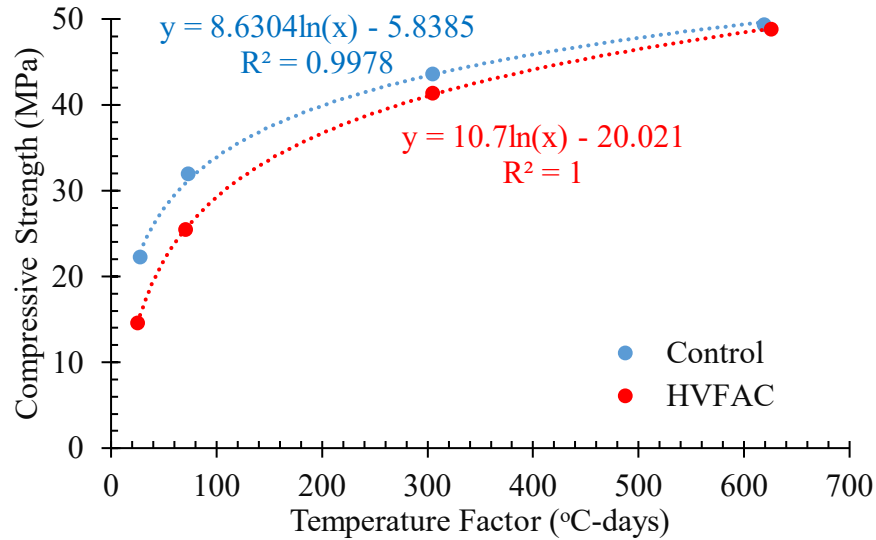


Figure 27. Graph. Laboratory maturity calibration curve for HVFAC and control mixes.

Source: Baral, Roesler, and Fu (2021)

### In-place Strength Estimation Using Maturity Method

In-place compressive strength can be determined from the maturity calibration curve. The in-place strength determined from the maturity calibration curve can be used to determine the earliest possible road-opening time. One of the variables in the field maturity calculation is the temperature data collection depth. Based on the in-place compressive strength estimation performed in the field test section, the compressive strength at the top and bottom of the slab as calculated using the maturity method was within 5% (Table 9). The percentage difference in the compressive strength between the top and the bottom of the slab was further reduced with increasing curing time. Thus, to evaluate the in-place compressive strength, the thermal sensor can be potentially placed at any depth for a concrete pavement less than 25.4 cm (10 in.) thickness.

Table 9. In-place Compressive Strength of the HVFAC Mix in the Field

	HVFAC Compressive Strength (MPa)			
	1.27 cm (0.5 in.)	7.62 cm (3 in.)	19.05 cm (7.5 in.)	22.86 cm (9 in.)
<b>Day 1</b>	16.1	16.6	16.6	16.6
<b>Day 2</b>	23.9	24.0	24.0	24.0
<b>Day 3</b>	27.9	28.3	28.4	28.4
<b>Day 14</b>	40.7	41.0	41.4	41.5
<b>Day 28</b>	47.5	47.7	48.0	48.1



## NONCONTACT ULTRASOUND SETTING TIME TEST METHOD

The noncontact ultrasound measurement device (Figure 28) developed by Tran and Roesler (2021) measures the energy of the leaky Rayleigh wave to determine concrete's final setting time in the field. The working principle of the noncontact ultrasound testing device (Tran and Roesler 2021) is described more in detail in the volume 2 report (Baral, Roesler, and Fu 2021). The evolution of the energy of the leaky Rayleigh wave over time for the concrete control and HVFAC mixes is shown in Figure 29. The noncontact ultrasound setting time device was successfully used to measure the final setting time of the control mix (4 hours 10 minutes) in the field. The final setting times determined from all three sensors were within 5 minutes. Because of the long setting time of the HVFAC mix, insufficient data was collected to predict the final set time (> 7 hours) in the field.

To further demonstrate the noncontact setting time device, the final setting time was measured in the lab environment for both the control and HVFAC mixture along with the calorimeter-based estimate of setting time. The calorimeter was run at 22°C (71.6°F), whereas the noncontact ultrasound setting time device was 25°C (77°F) in the lab environment. The final setting time obtained from these two testing methods is shown in Table 10. Both methods gave similar results for the same mix. The HVFAC mix had in the lab environment a very high final setting time of 14 to 15 hours, which was expected given the field results suggest it was much greater than 7 hours.

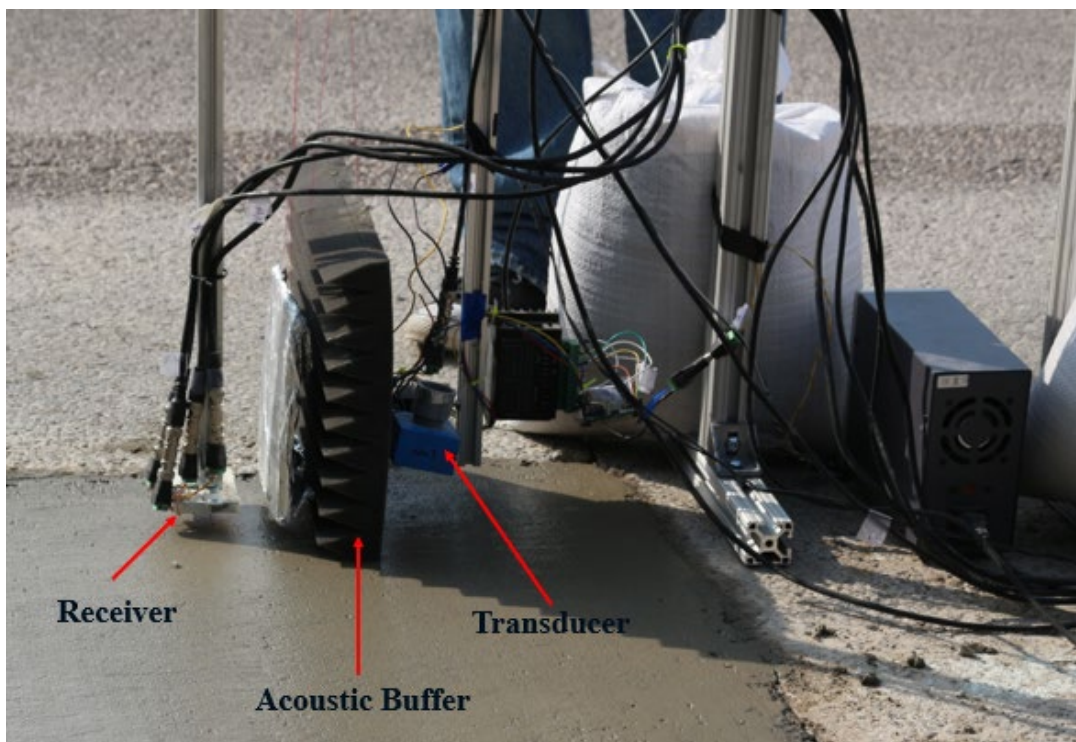
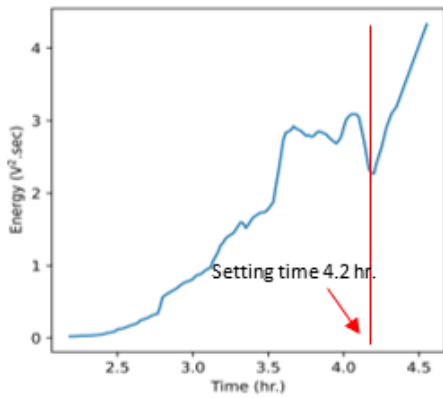
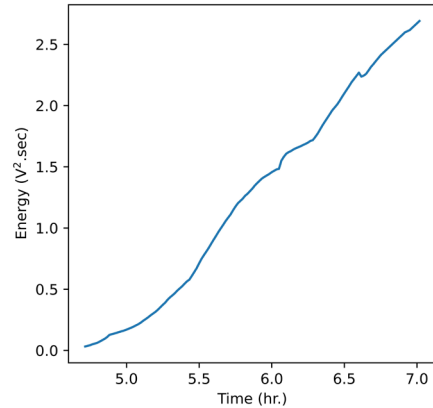


Figure 28. Photo. Noncontact ultrasound setting time measurement device at the field test site.

*Source: Baral, Roesler, and Fu (2021)*



A. Control mix



B. HVFAC mix

**Figure 29. Graphs. Leaky Rayleigh wave energy of the (a) control concrete and (b) HVFAC mixes.**

*Source: Baral, Roesler, and Fu (2021)*

**Table 10. Final Setting Time of HVFAC and Control Mixes in the Laboratory**

Mix Type	Noncontact Ultrasound	Calorimetry
Control	5.4 hours	5.7 hours
HVFAC	14 hours	15.2 hours

## SAW CUTTING

The optimal saw-cutting timing to minimize joint raveling, while ensuring joint activation without random crack development, is essential for long-term pavement performance. Recently, Tran and Roesler (2020) evaluated joint raveling at different times using a computer vision-based technique and concluded that the ideal saw-cutting time should be a function of the final setting time: Saw-cut time = 1.3 x Final Setting Time + 39 minutes. According to this formula, the saw-cutting time for the control mix should have been 6 hours 7 minutes from concrete casting. For the HVFAC mix, the final setting time in the field was greater than 7 hours, and thus the saw-cut timing should be at least 10 hours from concrete batching. As shown in Figure 30 saw cutting in both field test sections was performed too early (Control: 4 hr. 25 min; HVFAC: 5 hr. 35 min and 6 hr. 20 min), and severe joint raveling was observed in both the control and HVFAC sections. This reinforces the need for accurate final set time estimation to determine the saw-cut timing and avoidance of premature joint raveling.





A. Control mix: saw cut after 4 hours 25 minutes



B. HVFAC mix: saw cut after 5 hours 35 minutes



C. HVFAC mix: saw cut after 6 hours 20 minutes

**Figure 30. Photos. Saw cut and joint raveling in (a) control and (b and c) HVFAC sections.**

***Source: Baral, Roesler, and Fu (2021)***

## CHAPTER 5: MIX DESIGN ACCOMODATIONS FOR HVFAC

The workability, admixture dosage, setting time, and early-age strength gain can be challenging to predict with HVFAC. Thus, it is recommended to complete an oxide analysis of the fly ash; calorimeter tests of cement, fly ash, and admixtures; and a trial batch with all the expected constituent materials, proportions, and chemical admixtures. The adjustments discussed in this chapter should be first applied to an already approved traditional concrete mix design with lower fly ash content, e.g., 20% replacement. The maximum setting time limit, strength gain, and workability requirement of the HVFAC mix to be designed should be set before starting this mix design process. A HVFAC mix should not generally be used for concrete patching given the inherent early strength gain limitations of HVFAC, especially in the first 24 hours.

### STEP 1: OXIDE ANALYSIS AND STRENGTH PREDICTION

Bulk oxide content of the fly ash samples should be measured first using X-Ray Fluorescence (XRF). A web-based calculator was also developed to apply the bulk oxide contents to predicting various compressive strengths for higher volume fly ash ([www.tylerley.com/flyash](http://www.tylerley.com/flyash)). The calculator uses the bulk oxide content of the fly ash from a mill sheet or XRF to predict whether the fly ash will provide higher, lower, or the same performance as a mixture that only contains Portland cement. This prediction is made for both 20% and 40% fly ash replacement up to 180 days. The calculator's algorithm was developed based on 35 different fly ash samples and shows 90% accuracy. If the early-age predicted strength is higher or the same as the OPC mixes, then the next steps can be continued without accelerator or limestone replacement. Otherwise, accelerator addition, lowering of w/b ratio from the traditionally approved mix design, or limestone replacement should be considered to improve the setting time and early strength gain.

### STEP 2: AEA DOSAGE REQUIREMENT

Foam index or digital foam index tests on the fly ash sample should be performed. The AEA dosage requirement for achieving the 6% air content in concrete can be calculated from the foam index value, which was found for wood rosin-based AEA in this research. Similar relationships can be developed in the future for other AEAs.

### STEP 3: CALORIMETER RESPONSE

Calorimeter tests should be performed with the cement + fly ash + water + AEA + water reducer / superplasticizer mix. If limestone or an accelerator is added or lowering of w/b for strength gain enhancement in step 1, then those should also be followed in the calorimeter mix. The AEA dosage requirement obtained in step 2 should be used. The water reducer / superplasticizer target may need to be adjusted to accommodate reasonable setting times. In the case of extremely high and/or false setting, a different water reducer / superplasticizer may need to be considered.

## STEP 4: TRIAL MIX DESIGN AND ADJUSTMENTS

The preliminary mixture design should start with a typical concrete mixture design with fly ash and replace additional cement in the mixture with up to 40% fly ash by mass. The mixture should be initially adjusted to yield 0.764 m<sup>3</sup> (27 ft<sup>3</sup>) by adjusting the volume of the aggregates in the mixture to reflect the changes in volume of paste. The coarse and fine aggregates should both be adjusted to maintain the same coarse-to-fine aggregate proportions of the initial mix design. For example, if the fly ash content is increased relative to an existing replacement rate, e.g., from 25% to 40%, the fine aggregate content would decrease proportional to the change in volume of fly ash. Based on how IDOT calculates its concrete mix designs, in order to maintain the coarse-to-fine aggregate proportions of the 25% fly ash mix in the 40% fly ash mix, the mortar factor would need to increase (possibly by as little as 0.01). The water-to-binder ratio used in step 3 should be held constant in the mixture at the beginning, and the maximum possible water reducer / superplasticizer dosage determined in step 3 should be added. If the workability of this mix exceeds the required workability of the mix, then the water reducer / superplasticizer dosage can be reduced to obtain desired workability. If the workability of this mix does not meet required workability of the mix, then the water reducer / chemical admixture dosage needs to be increased to obtain desired workability. In that case, usage / increase in dosage of accelerator or limestone replacement must be considered to accelerate the setting time as measured using the calorimeter.

After the initial mixture constituents and proportions are selected for the HVFAC mixture, the following trial batch tests should be completed and checked with the specifications: slump, unit weight, air content, temperature, and compressive (and/or flexural) strength at 1, 3, 7, and 14 days. Longer ages may be beneficial to demonstrate the benefit of higher volume fly ash with time, e.g., 56 or 90 days. The strength testing at 1 and 3 days provides insight into the rate of strength gain of the HVFAC mixture. Embedded temperature sensors along with maturity calibration curves can estimate the field strength, which may be necessary for construction traffic or opening strength. The setting time of the HFVAC will depend on the temperature of the mixture and reaction kinetics. More exact methods for set time such as a penetration test on sieved mortar or ultrasonic set time measurement (Tran and Roesler 2021) can be done in the lab. Likewise, a small test section can be cast with workability, air, and strength cylinders sampled. This can also allow for set time determination and saw-cut timing with HVFAC mixtures.

Mixture adjustments based on the findings from the trial batch may be necessary. Table 11 gives recommendations on suggested changes to meet desired properties.

**Table 11. Mixture Property Adjustment Strategies for HVFAC Mixtures  
(Listed in Order of Importance)**

Property	Changes to make in the mixture
Workability	Water reducer dosage, water content, aggregate gradation
Air content	Air-entraining dosage
Set time	Accelerator, limestone powder, decrease w/cm

## CHAPTER 6: SUMMARY AND RECOMMENDATIONS

Implementation of concrete mixes with high supplementary cementitious materials content such as fly ash for concrete pavement construction can improve the cost, durability, and sustainability of the roadway. Despite these improvements, higher volume fly ash mixes can affect early-age properties such as workability, air entrainment, setting time, and strength gain. Previous researchers (Herath et al., 2020) have shown the durability of these higher volume fly ash mixes to be similar or better than conventional concrete. However, durability tests for freeze-thaw, ASR, and salt scaling should still be performed for verification because of potential adverse interactions between cement and fly ash sources coupled with chemical admixtures. In this research, five main areas were studied to assist in implementing higher volume fly ash mixes in concrete pavements.

First, early-age hydration and setting characteristics must be evaluated to avoid an unsatisfactory HVFA mixture, which can result in adverse reactions with undesirable setting times. Early-age hydration and setting times were successfully evaluated using isothermal calorimetry. The calorimeter can distinguish effects of different mix design variables such as chemical admixtures, fly ash sources, fly ash replacement levels, cement + fly ash interactions, and use of limestone powder to accelerate the setting time of HVFAC. Calorimeter testing demonstrated that certain cement–fly ash combinations or the addition of a chemical admixture (both PCE- and lignosulfonate-based) delayed the hydration of HVFAC. The PCE-based admixture gave the largest set time delays. Both nano- and micro-limestone replacement accelerated the final setting time, but the setting time acceleration was higher for nano-limestone replacement.

Second, to assist in maintaining the air content in HVFAC, the foam index test is necessary for monitoring the air-entraining dosage of HVFA concrete and checking the consistency of fly ash sources over time. As part of this research, a calibration curve between air-entraining dosage required for achieving 6% air content and foam index test was developed. To further improve the repeatability for a single operator and between labs, a computer vision–based digital foam index test was developed to make this test more widespread and consistent across multiple labs and operators.

Third, prediction models for the HVFAC compressive strength, resistivity, and diffusion coefficient were developed based on an oxide content–based particle model. A particle-based model can quickly help engineers predict these hardened properties without long-term testing, and thus immediate sensitivities are known for unexpected fly ash source changes.

Fourth, implementation of HVFAC in the field on concrete pavements requires procedures to determine the in situ final setting time and opening strength. The maturity method was successfully implemented with wireless thermal sensors to predict in-place compressive strength of HVFAC. Likewise, a noncontact ultrasound device was able to determine the final setting time in the lab and field for both control and HVFA concrete, which was used to indicate the earliest time to saw cut contraction joints to avoid joint raveling.

Fifth, a mix design procedure for HVFAC was proposed to adjust conventional concrete mixture for air content, workability, setting time, strength, and detection of potential adverse interactions of constituent materials through isothermal calorimetry.

Based on the research performed in this study, the following practices should be incorporated into IDOT's standard practices when using HVFAC.

- Calorimeter tests should be implemented on the cement, fly ash, and chemical admixture combination to be used in a project with HVHAC to measure setting times, peak heat flows, and cumulative heat flow.
- The compressive strength, resistivity, and diffusion should be estimated for HVFAC based on the oxide analysis and particle model to determine the early and long-term hardened properties relative to straight cement mixtures and 20% replacement mixtures.
- The digital foam index test or the foam index test should be implemented to determine the air-entraining dosage as required to achieve 6% air content for a HVFAC mixture. Additionally, the digital foam index should monitor the fly ash changes between quarterly samples and adjust air-entraining dosage for a new fly ash source or change in the air-entrainment admixture.
- After the initial oxide, calorimeter, and foam index tests, a trial batch procedure should be completed for a particular cement, fly ash, and chemical admixture combination to check the mix for target air content, workability, and early strengths.
- Noncontact ultrasonic device for determine the final setting time in the field should primarily be implemented to determine the saw-cut timing requirements, which can be determined as the following:  $\text{Saw-cut time} = 1.3 \times \text{Final Setting Time} + 39 \text{ minutes}$ . This minimum sawcut timing will limit joint raveling from developing because of too early cutting of contraction joints.
- The maturity method with wireless thermal sensors can be implemented for the determination of the opening strength time of HVFAC for construction and regular traffic. Furthermore, construction of HVFAC in cold weather should be monitored through the maturity method to ensure sufficient strength gain before opening the road to construction and regular traffic.
- HVFAC mixes for roadways should not be hand finished to minimize future salt-scaling damages.



## REFERENCES

- AASHTO R 80. 2017. *Standard Practice for Determining the Reactivity of Concrete Aggregates and Selecting Appropriate Measures for Preventing Deleterious Expansion in New Concrete Construction*. Washington, DC: AASHTO.
- AASHTO T 358. 2019. *Standard Method of Test for Surface Resistivity Indication of Concrete's Ability to Resist Chloride Ion Penetration*. Washington, DC: AASHTO.
- Aboustait, Mohammed, Taehwan Kim, M. Tyler Ley, and Jeffrey M. Davis. 2016. "Physical and Chemical Characteristics of Fly Ash Using Automated Scanning Electron Microscopy." *Construction and Building Materials* 106: 1–10. <https://doi.org/10.1016/j.conbuildmat.2015.12.098>.
- American Coal Ash Association. 2003. *Fly Ash Facts for Highway Engineers*. Aurora, CO: American Coal Ash Association.
- Andrade, Carmen, Renata d'Andrea, and Nuria Rebolledo. 2014. "Chloride Ion Penetration in Concrete: The Reaction Factor in the Electrical Resistivity Model." *Cement and Concrete Composites* 47: 41–46. <https://doi.org/10.1016/j.cemconcomp.2013.09.022>.
- ASTM C143/C143M. 2020. *Standard Test Method for Slump of Hydraulic-Cement Concrete*. West Conshohocken, PA: American Society for Testing and Materials. [https://doi.org/10.1520/C0143\\_C0143M-20](https://doi.org/10.1520/C0143_C0143M-20).
- ASTM C1556. 2016. *Standard Test Method for Determining the Apparent Chloride Diffusion Coefficient of Cementitious Mixtures by Bulk Diffusion*. West Conshohocken, PA: American Society for Testing and Materials.
- ASTM C1702. 2017. *Standard Test Method for Measurement of Heat of Hydration of Hydraulic Cementitious Materials Using Isothermal Conduction Calorimetry*. West Conshohocken, PA: American Society for Testing and Materials. <https://doi.org/10.1520/C1720-17>.
- ASTM C1827. 2020. *Standard Test Method for Determination of the Air-Entraining Admixture Demand of a Cementitious Mixture*. West Conshohocken, PA: American Society for Testing and Materials. <https://doi.org/10.1520/C1827-20>.
- ASTM C191. 2019. *Standard Practice for Mechanical Mixing of Hydraulic Cement Pastes and Mortars of Plastic Consistency*. West Conshohocken, PA: American Society for Testing and Materials.
- ASTM C305. 2020. *Standard Test Method for Compressive Strength of Cylindrical Concrete Specimens*. West Conshohocken, PA: American Society for Testing and Materials.
- ASTM C39. 2021. *Standard Test Method for Compressive Strength of Cylindrical Concrete Specimens*. West Conshohocken, PA: American Society for Testing and Materials.
- ASTM C403. 2016. *Standard Test Method for Time of Setting of Concrete Mixtures by Penetration Resistance*. West Conshohocken, PA: American Society for Testing and Materials. [https://doi.org/10.1520/C0403\\_C0403M-16](https://doi.org/10.1520/C0403_C0403M-16).
- ASTM C618. 2019. *Standard Specification for Coal Fly Ash and Raw or Calcined Natural Pozzolan for Use in Concrete*. West Conshohocken, PA: American Society for Testing and Materials.

<https://doi.org/10.1520/C0618-19>.

- Bamforth, P. B. 1980. "In Situ Measurement of the Effect of Partial Portland Cement Replacement Using Either Fly Ash or Ground Granulated Blast-Furnace Slag on the Performance of Mass Concrete." *Proceedings of the Institution of Civil Engineers (London). Part 1—Design & Construction* 69(pt 2): 777–800.
- Baral, Aniruddha, Jeffery R. Roesler, and Junryu Fu. 2021. *Early Age Properties of High Volume Fly Ash Concrete Mixes for Pavement: Volume 2*. Rantoul, IL: Illinois Center for Transportation. <https://doi.org/10.36501/0197-9191/21-031>
- Beckemeier, Karl Wehking. 2012. "Effects of High Volumes of FLY Ash on Cement Paste." Master's thesis, Missouri University of Science and Technology.
- Bentz, Dale P. 2011. "Powder Additions to Mitigate Retardation in High-Volume Fly Ash Mixtures." *ACI Materials Journal* (107): 508–14. <https://www.concrete.org/publications/internationalconcreteabstractsportal/m/details/id/51663971>.
- California Department of Transportation. 2013. *Concrete Technology Manual*. Sacramento, CA: California Department of Transportation. <https://dot.ca.gov/programs/engineering-services/manuals/sc-concrete-tech-manual>.
- Chen, Yuanzhi, Naresh Shah, Frank E. Huggins, Gerald P. Huffman, William P. Linak, and C. Andrew Miller. 2004. "Investigation of Primary Fine Particulate Matter from Coal Combustion by Computer-Controlled Scanning Electron Microscopy." *Fuel Processing Technology* 85 (6): 743–61. <https://doi.org/10.1016/j.fuproc.2003.11.017>.
- Detwiler, Rachel. 1997. *The Role of Fly Ash Composition in Reducing Alkali-Silica Reaction*. Skokie, IL: Portland Cement Association.
- Farnam, Yaghoob, Bochen Zhang, and Jason Weiss. 2017. "Evaluating the Use of Supplementary Cementitious Materials to Mitigate Damage in Cementitious Materials Exposed to Calcium Chloride Deicing Salt." *Cement and Concrete Composites* 81: 77–86. <https://doi.org/10.1016/j.cemconcomp.2017.05.003>.
- Federal Aviation Administration. 2018. "Advisory Circular 150/5370-10H Standard Specifications for Construction of Airports." Accessed August 2, 2020. [https://www.faa.gov/documentLibrary/media/Advisory\\_Circular/150-5370-10H.pdf](https://www.faa.gov/documentLibrary/media/Advisory_Circular/150-5370-10H.pdf)
- Ghosal, Sarbajit, Jon L. Ebert, and Sidney A. Self. 1995. "Chemical Composition and Size Distributions for Fly Ashes." *Fuel Processing Technology* 44 (1): 81–94. [https://doi.org/10.1016/0378-3820\(94\)00115-A](https://doi.org/10.1016/0378-3820(94)00115-A) .
- Gołaszewski, Jacek, Aleksandra Kostrzanowska-Siedlarz, Tomasz Ponikiewski, and Patrycja Miera. 2017. "Influence of Cements Containing Calcareous Fly Ash as a Main Component Properties of Fresh Cement Mixtures." *{IOP} Conference Series: Materials Science and Engineering* 245 (2): 22099. <https://doi.org/10.1088%2F1757-899x%2F245%2F2%2F022099>.
- Harris, Nathan J., Kenneth C. Hover, Kevin J. Folliard, and M. Tyler Ley. 2008a. "The Use of the Foam Index Test to Predict Air-Entraining Admixture Dosage in Concrete Containing Fly Ash: Part I—Development of a Standard Test Method: Proportions of Materials." *Journal of ASTM*

*International* 5 (7): 1–15.

- . 2008b. “The Use of the Foam Index Test to Predict Air-Entraining Admixture Dosage in Concrete Containing Fly Ash: Part II—Development of a Standard Test Method: Proportions of Materials.” *Journal of ASTM International* 5 (7): 1–15.
- . 2008c. “The Use of the Foam Index Test to Predict Air-Entraining Admixture Dosage in Concrete Containing Fly Ash: Part III—Development of a Standard Test Method: Proportions of Materials.” *Journal of ASTM International* 5 (7): 1–11.
- Herath, Charith, Chamila Gunasekara, David W. Law, and Sujeeva Setunge. 2020. “Performance of High Volume Fly Ash Concrete Incorporating Additives: A Systematic Literature Review.” *Construction and Building Materials*, 258: 120606. <https://doi.org/10.1016/j.conbuildmat.2020.120606>.
- Hu, Jiong, Zhi Ge, and Kejin Wang. 2014. “Influence of Cement Fineness and Water-to-Cement Ratio on Mortar Early-Age Heat of Hydration and Set Times.” *Construction and Building Materials* 50: 657–63. <https://doi.org/10.1016/j.conbuildmat.2013.10.011>.
- Hu, Qinang, M. Tyler Ley, Jeffrey Davis, Jay C. Hanan, Robert Frazier, and Yanli Zhang. 2014. “3D Chemical Segmentation of Fly Ash Particles with X-Ray Computed Tomography and Electron Probe Microanalysis.” *Fuel* 116: 229–36. <https://doi.org/10.1016/j.fuel.2013.07.037>.
- Hu, Qinang, Mohammed Aboustait, M. Tyler Ley, Jay C. Hanan, Volker Rose, and Robert Winarski. 2014. “Combined Three-Dimensional Structure and Chemistry Imaging with Nanoscale Resolution.” *Acta Materialia* 77: 173–82. <https://doi.org/10.1016/j.actamat.2014.05.050>.
- Jin, Shanshan, Zhang, Jinxi, and Huang, Baoshan. 2013. “Fractal Analysis of Effect of Air Void on Freeze-Thaw Resistance of Concrete.” *Construction and Building Materials* 47: 126–130. <https://doi.org/10.1016/j.conbuildmat.2013.04.040>.
- Kang, Shinhyu, M. Tyler Ley, and Amir Behravan. 2021. “Predicting Ion Diffusion in Fly Ash Cement Paste through Particle Analysis.” *Construction and Building Materials* 272: 121934. <https://doi.org/10.1016/j.conbuildmat.2020.121934>.
- Kang, Shinhyu, M. Tyler Ley, Zane Lloyd, and Taehwan Kim. 2020. “Using the Particle Model to Predict Electrical Resistivity Performance of Fly Ash in Concrete.” *Construction and Building Materials* 261: 119975. <https://doi.org/10.1016/j.conbuildmat.2020.119975>.
- Kang, Shinhyu, Zane Lloyd, Amir Behravan, and M. Tyler Ley. 2021. “The Relationship between the Apparent Diffusion Coefficient and Surface Electrical Resistivity of Fly Ash Concrete.” *Construction and Building Materials* 299: 123964. <https://doi.org/10.1016/j.conbuildmat.2021.123964>.
- Kang, Shinhyu, Zane Lloyd, Taehwan Kim, and M. Tyler Ley. 2020. “Predicting the Compressive Strength of Fly Ash Concrete with the Particle Model.” *Cement and Concrete Research* 137: 106218. <https://doi.org/10.1016/j.cemconres.2020.106218>.
- Kim, T., M. Moradian, and M. Tyler Ley. 2018. “Dissolution and Leaching of Fly Ash in Nitric Acid Using Automated Scanning Electron Microscopy.” *Advances in Civil Engineering Materials* 7 (1): 291–307. <https://doi.org/10.1520/ACEM20180016>.
- Kim, Taehwan, Jeffrey M. Davis, M. Tyler Ley, Shinhyu Kang, and Pouya Amrollahib. 2018. “Fly Ash



- Particle Characterization for Predicting Concrete Compressive Strength.” *Construction and Building Materials* 165: 560–71. <https://doi.org/10.1016/j.conbuildmat.2018.01.059>.
- Kim, Taehwan, M. Tyler Ley, Shinyu Kang, Jeffrey M. Davis, Seokhyeon Kim, and Pouya Amrollahib. 2020. “Using Particle Composition of Fly Ash to Predict Concrete Strength and Electrical Resistivity.” *Cement and Concrete Composites* 107 (September 2019): 103493. <https://doi.org/10.1016/j.cemconcomp.2019.103493>.
- Kutchko, Barbara G., and Ann G. Kim. 2006. “Fly Ash Characterization by SEM–EDS.” *Fuel* 85 (17): 2537–44. <https://doi.org/10.1016/j.fuel.2006.05.016>.
- Ley, M. Tyler, Nathan J. Harris, Kevin J. Folliard, and Kenneth C. Hover. 2008. “Investigation of Air-Entraining Admixture Dosage in Fly Ash Concrete.” *ACI Materials Journal* 105 (5): 494–98.
- Ley, M. Tyler, Z. Lloyd, S. Kang, and D. Cook. 2021. *Concrete Pavement Mixtures with High Supplementary Cementitious Materials (SCM) Content: Volume 3*. Rantoul, IL: Illinois Center for Transportation. <https://doi.org/10.36501/0197-9191/21-032>.
- Liu, Yanbo, Francisco J. Presuel-Moreno, and Mario A. Paredes. 2015. “Determination of Chloride Diffusion Coefficients in Concrete by Electrical Resistivity Method.” *ACI Materials Journal* 112(5).
- Nassif, Hani, and Nakin Suksawang. 2003. *Development of High-Performance Concrete for Transportation Structures in New Jersey*. Rutgers: NJ: Center for Advanced Infrastructure & Transportation. <https://www.nj.gov/transportation/business/research/reports/FHWA-NJ-2003-016.pdf>.
- Öztürk, T., O. Kroggel, P. Grübl, and J. S. Popovics. 2006. “Improved Ultrasonic Wave Reflection Technique to Monitor the Setting of Cement-Based Materials.” *NDT & E International* 39 (4): 258–63. <https://doi.org/10.1016/j.ndteint.2005.06.012>.
- Reinhardt, H. W., C. U. Große, and A. T. Herb. 2000. “Ultrasonic Monitoring of Setting and Hardening of Cement Mortar—A New Device.” *Materials and Structures* 33 (9): 581–83. <https://doi.org/10.1007/BF02480539>.
- Ryan, Eric, Edwin Burdette, Ryan Ankabrandt, Robert Nidiffer, and Brian Buchanan. 2014. “Comparison of Two Methods to Assess the Resistance of Concrete to Chloride Ion Penetration.” *Journal of Materials in Civil Engineering* 26 (4): 698–704. [https://doi.org/10.1061/\(ASCE\)MT.1943-5533.0000844](https://doi.org/10.1061/(ASCE)MT.1943-5533.0000844).
- Suraneni, Prannoy, Vahid J. Azad, O. Burkan Isgor, and W. Jason Weiss. 2017. “Use of Fly Ash to Minimize Deicing Salt Damage in Concrete Pavements.” *Transportation Research Record* 2629 (2629): 24–32.
- Tang, L. 2008. *Guideline for Practical Use of Methods for Testing the Resistance of Concrete to Chloride Ingress*. Borås, Sweden: SP Swedish National Testing and Research Institute.
- Tanikella, Prasanth, and Jan Olek. 2017. *Updating Physical and Chemical Characteristics of Fly Ash for Use in Concrete*. West Lafayette, IN: Joint Transportation Research Program.
- Taylor, Peter, Luis A. Graf, Jerzy Z. Zemajtis, Vagn C. Johansen, Ronald L. Kozikowski, and Chiara F. Ferraris. 2006a. *Identifying Incompatible Combinations of Concrete Materials: Volume I—Final*

Report. Washington, DC: Federal Highway Administration. <https://rosap.ntl.bts.gov/view/dot/727>.

———. 2006b. *Identifying Incompatible Combinations of Concrete Materials: Volume II—Test Protocol*. Washington, DC: Federal Highway Administration.

Tran, Quang, and Jeffery R. Roesler. 2020. “Noncontact Ultrasonic and Computer Vision Assessment for Sawcut Initiation Time.” *Journal of Transportation Engineering, Part B: Pavements* 146 (3): 04020055.

———. 2021. “Contactless Ultrasonic Test System for Set Times of Mortar and Concrete.” *ACI Materials Journal* 118 (2). <https://doi.org/10.14359/51729328>.

Xiao, Lianzhen, Zheng Ren, Wenchong Shi, and Xiaosheng Wei. 2016. “Experimental Study on Chloride Permeability in Concrete by Non-Contact Electrical Resistivity Measurement and RCM.” *Construction and Building Materials* 123: 27–34. <https://doi.org/10.1016/j.conbuildmat.2016.06.110>.

Yurdakul, Ezgi, Peter C. Taylor, Halil Ceylan, and Fatih Bektas. 2014. “Effect of Water-to-Binder Ratio, Air Content, and Type of Cementitious Materials on Fresh and Hardened Properties of Binary and Ternary Blended Concrete.” *Journal of Materials in Civil Engineering* 26 (6). [https://doi.org/10.1061/\(ASCE\)MT.1943-5533.0000900](https://doi.org/10.1061/(ASCE)MT.1943-5533.0000900).



**I** ILLINOIS